






A Bias-free Cosmological Analysis with Quasars Alleviating H_0 Tension

Aleksander Łukasz Lenart^{1,11}, Giada Bargiacchi^{2,3,11} , Maria Giovanna Dainotti^{4,5,6} , Shigehiro Nagataki^{7,8,9}, and Salvatore Capozziello^{2,3,10} 

¹ Astronomical Observatory, Jagiellonian University, ul. Orła 171, 31-501 Kraków, Poland

² Scuola Superiore Meridionale, Largo S. Marcellino 10, I-80138, Napoli, Italy; giada.bargiacchi@unina.it

³ Istituto Nazionale di Fisica Nucleare (INFN), Sez. di Napoli, Complesso Univ. Monte S. Angelo, Via Cinthia 9, I-80126, Napoli, Italy

⁴ National Astronomical Observatory of Japan, 2 Chome-21-1 Osawa, Mitaka, Tokyo 181-8588, Japan

⁵ The Graduate University for Advanced Studies, SOKENDAI, Shonankokusaimura, Hayama, Miura District, Kanagawa 240-0193, Japan

⁶ Space Science Institute, 4765 Walnut Street, Suite B, Boulder, CO 80301, USA

⁷ Interdisciplinary Theoretical & Mathematical Science Program, RIKEN (iTHEMS), 2-1 Hirosawa, Wako, Saitama, 351-0198, Japan

⁸ RIKEN Cluster for Pioneering Research, Astrophysical Big Bang Laboratory (ABBL), 2-1 Hirosawa, Wako, Saitama, 351-0198, Japan

⁹ Astrophysical Big Bang Group (ABBG), Okinawa Institute of Science and Technology Graduate University (OIST), 1919-1 Tancha, Onna-son, Kunigami-gun, Okinawa, 904-0495, Japan

¹⁰ Dipartimento di Fisica “E. Pancini,” Università degli Studi di Napoli “Federico II,” Complesso Univ. Monte S. Angelo, Via Cinthia 9 I-80126, Napoli, Italy

Received 2022 September 22; revised 2022 November 15; accepted 2022 November 16; published 2023 February 6

Abstract

Cosmological models and their parameters are widely debated because of theoretical and observational mismatches of the standard cosmological model, especially the current discrepancy between the value of the Hubble constant, H_0 , obtained by Type Ia supernovae (SNe Ia), and the cosmic microwave background radiation (CMB). Thus, considering high-redshift probes like quasars (QSOs), having intermediate redshifts between SNe Ia and CMB, is a necessary step. In this work, we use SNe Ia and the most updated QSO sample, reaching redshifts up to $z \sim 7.5$, applying the Risaliti–Lusso QSO relation based on a nonlinear relation between ultraviolet and X-ray luminosities. We consider this relation both in its original form and corrected for selection biases and evolution in redshift through a reliable statistical method also accounting for the circularity problem. We also explore two approaches: with and without calibration on SNe Ia. We then investigate flat and nonflat standard cosmological models and a flat w CDM model, with a constant dark energy equation-of-state parameter w . Remarkably, when correcting for the evolution as a function of cosmology, we obtain closed constraints on Ω_M using only noncalibrated QSOs. We find that considering noncalibrated QSOs combined with SNe Ia and accounting for the same correction, our results are compatible with a flat Λ CDM model with $\Omega_M = 0.3$ and $H_0 = 70 \text{ km s}^{-1} \text{ Mpc}^{-1}$. Intriguingly, the H_0 values obtained are placed halfway between the one from SNe Ia and CMB, paving the way for new insights into the H_0 tension.

Unified Astronomy Thesaurus concepts: [Quasars \(1319\)](#); [Cosmological parameters \(339\)](#); [Dark energy \(351\)](#); [Cosmology \(343\)](#); [Cosmological models \(337\)](#)

1. Introduction

Quasars (QSOs) are extraordinarily luminous active galactic nuclei currently observed up to redshift $z = 7.642$ (Wang et al. 2021). These features make them potentially the next rung of the cosmic distance ladder beyond Type Ia supernovae (SNe Ia) that have been observed only up to $z = 2.26$ (Rodney et al. 2015). Using QSOs as cosmological tools requires a full understanding of their physical mechanisms that are still being debated by the scientific community.

A nonlinear relation between the ultraviolet (UV) and X-ray luminosities in QSOs was first discovered by the first X-ray surveys (Tananbaum et al. 1979; Zamorani et al. 1981; Avni & Tananbaum 1986), and has been confirmed using various samples of QSOs observed with the main X-ray observatories over a wide redshift range and wide ranges of UV luminosity that span over 5 orders of magnitudes (e.g., Steffen et al. 2006; Just et al. 2007; Lusso et al. 2010; Lusso & Risaliti 2016;

Bisogni et al. 2021). One possible physical explanation of this relation is as follows: QSO accretion disk on a central supermassive black hole emits photons in the UV band, which are then processed through the inverse Compton effect by an external plasma of relativistic electrons, giving rise to the X-ray emission. This physical explanation, while plausible, lacks accounting for the stability of the X-ray emission, as the external electrons should cool down due to the inverse Compton effect and fall onto the central region. Ultimately, one needs an efficient energy transfer between the accretion disk and the external region to describe such a stable emission. The nature of this link between the two regions is not known yet. However, some models have been proposed (see, e.g., Lusso & Risaliti 2017).

This X–UV relation has been recently used to provide independent measurements of QSO distances (see, e.g., Risaliti & Lusso 2015, 2019; Lusso et al. 2020, for details) making them standardized cosmological tools. In its cosmological application, this relation is referred to as the Risaliti–Lusso (RL) relation. To use this relation in cosmology, we need to properly select the QSO sample addressing as many observational issues as possible, such as dust reddening, X-ray absorption, galaxy contamination, and Eddington bias, as specified in Lusso et al. (2020) and Dainotti et al. (2022a).

¹¹ The first and second authors share the same contribution.



Indeed, in its first applications, the X–UV relation showed a very large intrinsic dispersion $\sigma_V \sim 0.35/0.40$ dex in logarithmic units (Lusso et al. 2010). Only recently has it been discovered that this dispersion is not completely intrinsic, but has mainly an observational origin (Lusso & Risaliti 2016); thus, an accurate selection of the sources is crucial. This finding has allowed reducing the intrinsic scatter to $\sigma_V \sim 0.2$ dex (Lusso et al. 2020) and has rendered this relation suitable for cosmological analyses, turning QSOs into more reliable cosmological tools. In addition, Dainotti et al. (2022a) proved through well-established statistical tests that this relation is not induced or distorted by selection biases and/or redshift evolution, but it is intrinsic to the physics of QSOs. The methodology used to standardize QSOs is complementary to the one traditionally applied for SNe Ia to estimate the cosmological parameters, yet it extends the Hubble–Lemaître diagram (i.e., the distance modulus–redshift diagram) to a redshift range currently inaccessible to SNe Ia ($z = 2.26\text{--}7.54$). Indeed, extending the cosmological computations with high-redshift data is crucial to distinguish between different cosmological models that are degenerate at low redshifts, to allow for better constraints on the dark energy (DE) behavior, and to explore possible extensions of the standard cosmological model.

As a matter of fact, the most widely adopted parameterization of the observed universe is based on the so-called Λ CDM model (Peebles 1984), which relies on the existence of cold dark matter (CDM) and DE (Λ) associated with a cosmological constant (Carroll 2001) in a spatially flat geometry. Predictions from this model have been found to agree with most of the observational probes such as the cosmic microwave background (CMB; e.g., Planck Collaboration et al. 2020), the baryon acoustic oscillations (BAOs; e.g., Alam et al. 2021), and the present accelerated expansion of the Hubble flow, based on the Hubble–Lemaître diagram of SNe Ia (e.g., Riess et al. 1998; Perlmutter et al. 1999), where the dominant dynamical contribution of DE related to the cosmological constant should drive such an acceleration. However, the fundamental physical origin and the properties of DE are still unknown, as the interpretation of Λ is hampered by a severe fine-tuning issue to obtain the right amount of DE observed today. Moreover, the data sets mentioned above do not fully exclude a spatially nonflat universe (Park & Ratra 2019; Di Valentino et al. 2020, 2021; Handley 2021; Yang et al. 2021). Relevant deviations from the spatially flat Λ CDM model have already been found using high-redshift probes; Dainotti et al. (2008, 2011, 2013a, 2020a, 2020b, 2022c) worked extensively on the standardization of gamma-ray bursts (GRBs) as cosmological candles, while QSOs combined with SNe Ia have been studied by Risaliti & Lusso (2019), Lusso et al. (2019, 2020), and Bargiacchi et al. (2021, 2022).

In addition, the search for high-redshift standard candles has also been enhanced by the Hubble tension, a $4\sigma\text{--}6\sigma$ discrepancy between the direct measurements of the local Hubble constant H_0 and the one inferred from cosmological models, remarkably the value from the Planck data based on the CMB within the Λ CDM model. The restricted number of cosmological probes at intermediate redshifts and selection biases are the major shortcomings that prevent a solution to this problem. Thus, additional high- z standardized probes beyond SNe Ia, such as GRBs and QSOs, could be instrumental in shedding light on this problem (Cardone et al. 2009, 2010;

Postnikov et al. 2014; Benetti & Capozziello 2019; Capozziello & D’Agostino 2020; Capozziello et al. 2020; Bargiacchi et al. 2021, 2022; Dainotti et al. 2021b, 2022b, 2022d; Moresco et al. 2022). Several groups worldwide are investigating if this tension is due to selection biases, or due to new physics. The H_0 tension is mainly discussed within the Λ CDM model, characterized by a constant equation of state of DE ($w = -1$), but it is vital to investigate the extensions of this model, such as the w CDM model, in which $w \neq -1$, or nonflat models. Relaxing the standard Λ CDM model, rigorously flat in spatial curvature and with nonevolving Λ , is conceptually useful both for solving the cosmological constant problem and as a possible arena for new physics asking for the evolution of DE (Perivolaropoulos 2014; Capozziello et al. 2019; Perivolaropoulos & Kazantzidis 2019; Perivolaropoulos & Skara 2021, 2022).

Therefore, we here conduct a detailed analysis of both of these extensions of the flat Λ CDM model using QSOs, through the RL relation, and SNe Ia as cosmological probes. For the first time in the literature, the so-called circularity problem can be solved for QSOs corrected for evolutionary effects. The circularity means that the computations of cosmological parameters depend on the underlying the cosmological model assumed, and hence this implies the assumption of given cosmological parameters. In general the parameters of correlations depend on values of cosmological parameters if they involve the luminosities or energies, thus fixed parameters of the correlations obtained under the assumption of some cosmological model, would bias cosmological results computed with such fixed parameters. This work shows important points of originality compared to previous analyses based on QSOs (e.g., Risaliti & Lusso 2015, 2019; Khadka & Ratra 2020a, 2020b; Lusso et al. 2020; Bargiacchi et al. 2021, 2022; Colgáin et al. 2022): (1) we apply the RL relation not only in its original form, the one commonly used for cosmological studies, but we also take into account selection biases and the evolution in redshift of the luminosities through reliable statistical methods overcoming the so-called circularity problem; (2) we investigate how cosmological results change upon the choice of calibrating or noncalibrating QSOs with SNe Ia; and (3) we discuss how the H_0 tension will be impacted by the inclusion of QSOs in the analyses and to what extent nonflat cosmological models can be a viable explanation for describing the current results. Our point of view is empirical and conservative and shows that improving data samples and distance indicators, first of all in the redshift range between SNe Ia and CMB, could alleviate the H_0 tension.

Recent studies have investigated the reliability of the application of the X–UV relation in cosmology. In Petrosian et al. (2022), the authors argued that the RL procedure is circular. In this work, we completely overcome, for the first time in the literature on QSOs, the circularity problem while also accounting for the correction for evolution in redshift of luminosities. Indeed, we apply this correction contemporaneously to the variation of cosmological parameters, as detailed in Section 3.2. Moreover, the authors of the above-mentioned paper base their criticism on a binned analysis of the parameters of the RL relation, which is not an appropriate approach due to the relative large dispersion of the correlation. Although we agree that without correcting the relation there exists a clustering of data points in relation to the redshift, as shown in the left panel of Figure 1, we overcome this issue by

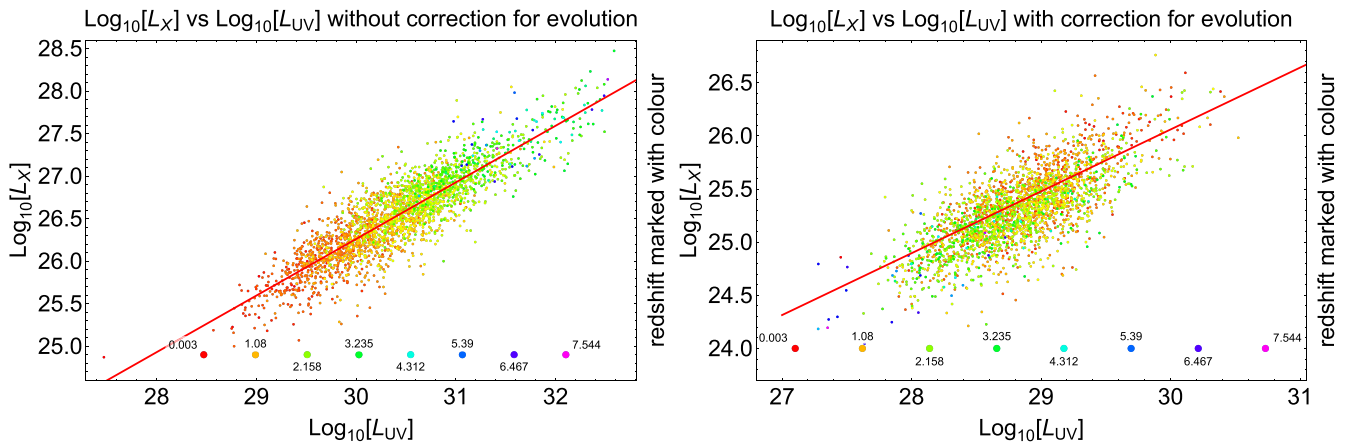


Figure 1. Comparison of the RL relation with and without the correction for evolution in redshift of luminosities, as shown in the right and left panels, respectively. Points are marked with different colors according to their redshift, as depicted in the pictures, and the red line represents the best-fit linear RL relation.

applying the correction for redshift evolution and selection biases, as visible in the right panel of the same figure. Thus, we agree that one cannot apply calibration methodology in a simple straightforward way without any correction. Our results presented in this article show that calibration methodology becomes unnecessary in many cases, when our innovative approach is applied, but we still show results of the calibration methodology without the correction, for the sake of comparison on how our correction changes the results. Indeed, in this article, we show that QSOs have a high potential to be standalone cosmological probes. From another point of view, Khadka & Ratra (2021, 2022) doubted the applicability of the QSO sample in its entirety for constraining cosmological parameters stating that the parameters of the RL relation depend on the cosmological model assumed and the redshift. Khadka & Ratra (2021, 2022) stated that due to those issues, some QSO subsamples cannot be standardized. Thus, their effort is in the direction of pinpointing a subsample with a higher potential for standardizing QSOs. Our approach is different, and we focus on the correction of the whole sample in order to use its full potential of extending the Hubble diagram. We agree that the noncorrected RL relation is changing with redshift, and we solve this issue further in the article. Conversely, we here find compatibility in 1σ (except for one case with a 2σ discrepancy) between the values of all of the parameters of the relation when using noncalibrated QSOs combined with SNe Ia, independently of the model studied. Khadka & Ratra (2021, 2022) found incompatibility in more than 3σ only in very exotic models. Moreover, our correction for selection bias and redshift evolution, treated as a function of evolution, leads to the compatibility of all parameters in less than 0.2σ . These results are shown and discussed in Sections 5.2–5.4. Thus, these discussions on the RL relation and its applicability are not a concern given our innovative approach and results.

The article is organized as follows. In Section 2 we present the data sets used for the cosmological analyses and their selection, and in Section 3 we present the methodology applied for the fits and the treatment of selection biases, redshift evolution of luminosities, circularity problem, and calibration of QSOs. In Section 4 we describe the cosmological models studied in this work and our assumptions on their corresponding parameters, while in Section 5 we present the main results for all data sets and different approaches comparing

them and discussing the implications. Finally, in Section 6, we summarize our findings.

2. The Data

Here, we work by selecting and combining samples of QSO and SNe Ia measurements to investigate the late-time universe. In this section, we describe each data set used for the cosmological analyses. These are carried out using both QSOs alone and the two probes combined.

For SNe Ia, we consider the collection of 1048 sources from the *Pantheon* sample (Scolnic et al. 2018). These are collected by different surveys and span from $z = 0.01$ up to $z = 2.26$. The sample of QSOs used is the one described in Lusso et al. (2020). This is composed of 2421 sources that cover the redshift range up to $z = 7.54$ (Bañados et al. 2018). These sources have been carefully selected for cosmological studies, and we refer the reader to the detailed descriptions in Risaliti & Lusso (2015, 2019), Lusso & Risaliti (2016), Salvestrini et al. (2019), and Lusso et al. (2020). Here and in Section 3.1, we summarize the crucial points required by the present work.

This QSO sample is properly selected to remove as many observational biases as possible. First, a selection is made by removing the sources for which the signal-to-noise ratio (S/N) does not guarantee well-sampled photometry (i.e., $S/N < 1$). After this first screening, all QSOs with a spectral energy distribution (SED) that shows UV reddening and near-infrared host-galaxy contamination are discarded, requiring only sources with extinction $E(B - V) \leq 0.1$. This corresponds to selecting only the sources that satisfy $\sqrt{(\Gamma_{1,UV} - 0.82)^2 + (\Gamma_{2,UV} - 0.40)^2} \leq 1.1$, where $\Gamma_{1,UV}$ and $\Gamma_{2,UV}$ are the slopes of a $\log(\nu)$ – $\log(\nu L_\nu)$ power law in the rest frame 0.3 – $1 \mu\text{m}$ and 1450 – 3000 \AA ranges, respectively, and ν and L_ν are the frequency and the luminosity per unit of frequency. The values $\Gamma_{1,UV} = 0.82$ and $\Gamma_{2,UV} = 0.4$ refer to an SED with zero extinction (see Richards et al. 2006). In addition, X-ray observations where photon indices (Γ_X) are peculiar or indicative of absorption are excluded by requiring $\Gamma_X + \Delta\Gamma_X \geq 1.7$ and $\Gamma_X \leq 2.8$ if $z < 4$ and $\Gamma_X \geq 1.7$ if $z \geq 4$, where $\Delta\Gamma_X$ is the uncertainty on the photon index. Finally, the remaining observations are corrected for the Eddington bias. Indeed, the cleaned sample consists only of sources fulfilling $\log F_{X,exp} - \log F_{min} \geq \mathcal{F}$, where \mathcal{F} is a threshold value, and $F_{X,exp}$ is the X-ray flux computed from the observed UV flux assuming the RL relation with fixed parameters within the flat ΛCDM model with $\Omega_M = 0.3$ and $H_0 = 70 \text{ km s}^{-1} \text{ Mpc}^{-1}$. F_{lim}

is the flux limit of the specific observation estimated from the catalog. More precisely, as detailed in Lusso & Risaliti (2016), for each object the minimum detectable flux is computed from the total exposure time of the charge-coupled device where the source is detected using the functions plotted in Figure 3 by Watson et al. (2001). The value of \mathcal{F} required in this filter is $\mathcal{F} = 0.9$ for the Sloan Digital Sky Survey Data (SDSS) Release 14 (DR14)–4XMM Newton (P aris et al. 2018; Webb et al. 2020) and XXL (Menzel et al. 2016) subsamples and $\mathcal{F} = 0.5$ for the SDSS-Chandra (Evans et al. 2010). All of the surviving multiple X-ray observations are ultimately averaged to reduce the effects of the X-ray variability. The sample we use is the result of all of these selection filters.

Here, we also remark that, as opposed to what has been done by other authors (e.g., Lusso et al. 2020; Bargiacchi et al. 2021, 2022), we consider the full sample of QSOs, without the filter of $z > 0.7$ proposed in Lusso et al. (2020), thus highlighting that the results shown here are not biased by any cut in redshift in the sample nor suffer from artificial truncation of the current data sample. In addition, this QSO sample is the most suitable one for cosmological studies, compared to others previously used in the literature (see, e.g., Risaliti & Lusso 2015, 2019; Singal et al. 2016; Lusso et al. 2019), for several reasons: (1) it is obtained by matching recent UV and X-ray surveys (e.g., SDSS DR14, 4XXM Newton), (2) it is carefully analyzed and selected against observational biases (Lusso et al. 2020), (3) it presents observations of 29 luminous QSOs in the high-redshift range of $z = 3.0\text{--}3.3$, which have been obtained from an XMM-Newton campaign (cycle 16, proposal ID: 080395, PI: Risaliti), and had been specifically selected as suitable for cosmological analyses because they represented the most luminous QSO population with homogeneous optical/UV properties (Nardini et al. 2019), and (4) it includes two samples of $z > 4$ QSOs published by Salvestrini et al. (2019) and Vito et al. (2019) and a local sample in the redshift range $0.009 < z < 0.1$. These factors guarantee a high quality of measurements, a huge number of sources, high-redshift points to extend the Hubble–Lema tre diagram far beyond the one of SNe Ia, and coverage at very low- z that allows for a better calibration with SNe Ia.

3. Methodology

3.1. Fitting Methodology

All of the analyses presented in this work are obtained using our own codes in Mathematica 12.2 (Wolfram Research, Inc., 2021) and Jupyter notebooks (Kluyver et al. 2016), in which we computed the investigated parameters using a Bayesian technique, the D’Agostini method (D’Agostini 2005). This technique makes use of Markov Chain Monte Carlo (MCMC) approach. The D’Agostini method has the advantage of accounting for error bars on both variables considered and also for an intrinsic dispersion sv of the relation fitted. Our applied algorithm starts from a given uniform prior of the parameters. Then the algorithms search in a loop for solutions of values of the parameters within the priors that maximize the likelihood. With every iteration of the loop, the priors are updated, remembering previous results based on the application of Bayes’ theorem. With this technique we can obtain a distribution of probabilities of all parameters at once without fixing any of them. This allows us to overcome the circularity problem without the aid of any calibrator.

The likelihood function (LF) used in this method to fit the SNe Ia sample is defined as¹²

$$\ln(\text{LF})_{\text{SNe}} = -\frac{1}{2}[(\mathbf{y} - \boldsymbol{\mu})^T C^{-1}(\mathbf{y} - \boldsymbol{\mu})] \quad (1)$$

where \mathbf{y} is the distance modulus measured, C is the associated 1048×1048 covariance matrix that includes both statistical and systematic uncertainties, and $\boldsymbol{\mu}$ is the distance modulus predicted by the cosmological model assumed, yet depending both on the free parameters of the model and the redshift.

As anticipated, the strategy to compute QSO distances makes use of the nonlinear relation between their UV and X-ray luminosity (Steffen et al. 2006; Just et al. 2007; Lusso et al. 2010; Lusso & Risaliti 2016; Bisogni et al. 2021), namely

$$\log L_X = g \log L_{\text{UV}} + b \quad (2)$$

where L_X and L_{UV} are the luminosities (in $\text{erg s}^{-1} \text{Hz}^{-1}$) at 2 keV and 2500  , respectively. In Dainotti et al. (2022a), this relation has been corrected for selection biases and redshift evolution using the Efron & Petrosian method (Efron & Petrosian 1992, hereafter EP), and it has been proved that it is intrinsic to QSO’s properties so that it can be reliably used to standardize QSOs as cosmological tools. To make use of Equation (2), we compute luminosities from measured flux densities F according to $L_{X,\text{UV}} = 4\pi d_l^2 F_{X,\text{UV}}$, where d_l is the luminosity distance. d_l is computed under the assumption of a cosmological model using the corresponding parameters as free parameters of the fit. Usually, luminosities of the sources have to be corrected for the K -correction, defined as $1/(1+z)^{1-\alpha}$, where α is the spectral index of the sources, but for QSOs it is assumed to be $\alpha = 1$, leading to a $K = 1$. So the K -correction has been omitted following Lusso et al. (2020). The LF function used for QSOs is (see also Khadka & Ratra 2021, 2022; Bargiacchi et al. 2022; Colg ain et al. 2022):

$$\ln(\text{LF})_{\text{QSO}} = -\frac{1}{2} \sum_{i=1}^N \left[\frac{(y_i - \phi_i)^2}{s_i^2} + \ln(s_i^2) \right]. \quad (3)$$

In this case, the data y_i correspond to $\log L_X$, while ϕ_i corresponds to the logarithmic X-ray luminosity predicted by the X–UV relation. Moreover, $s_i^2 = \sigma_y^2 + g^2 \sigma_x^2 + sv^2$, and it takes into account the statistical uncertainties on $\log L_X$ (y) and $\log L_{\text{UV}}$ (x), but also the intrinsic dispersion sv of the X–UV relation, which is another free parameter of the fit. Practically, LF_{QSO} is just the same LF function used for SNe Ia in Equation (1), but modified to include the contribution of the intrinsic dispersion of the X–UV relation. In all models studied in this work, we fit also QSOs combined with SNe Ia; thus, the joint LF function used for the combined sample of QSOs and SNe Ia is given by $\ln(\text{LF})_{\text{QSO+SNe}} = \ln(\text{LF})_{\text{SNe}} + \ln(\text{LF})_{\text{QSO}}$. In this work, we explore different methods to apply the QSO relation to cosmology. Specifically, we use (i) Equation (2) in its form, (ii) Equation (2) corrected for a fixed evolution in redshift of luminosities, and (iii) Equation (2) corrected for a redshift evolution of luminosities that varies together with cosmological parameters. For each of these approaches, we

¹² For the sake of simplicity, we always use \ln instead of \log_e and \log instead of \log_{10} .

also consider two different cases: with and without calibration with SNe Ia. Details of all of these different approaches are given in the following subsections.

3.2. Selection Biases and Redshift Evolution with a Circularity-free Treatment

As already stressed, QSOs are observed at very high redshifts, which is their huge advantage for cosmological applications, but also the reason for significant selection biases. Indeed, as it has been pinpointed in astrophysics, such selection biases can deform a correlation between the physical parameters of a source (see Figure 1), distort the cosmological parameters (Dainotti et al. 2013a), or even induce an artificial correlation. Thus, it is vital to test correlations against this type of effects.

The most commonly used method to correct data for selection biases and redshift evolution is the EP method, whose reliability has already been demonstrated for GRBs, also via Monte Carlo simulations (see, e.g., Dainotti et al. 2013a, 2013b, 2015, 2017, 2021a). This method assumes that the corrected, de-evolved, physical quantity (in our case the luminosity) L' is equal to the observed one L divided by some function of the redshift $\xi(z)$ of an assumed form, $L' = \frac{L}{\xi(z)}$. The simplest function that mimics the evolution is the power law $\xi(z) = (1+z)^k$ (see, e.g., Dainotti et al. 2013a, 2017). As addressed in Dainotti et al. (2015), the functional form for the evolution can be a power law of this form or a more complex function (see also Singal et al. 2011), but both of these functions result in computed parameters that are compatible in 1σ for the case of QSOs (see Table 1 of Dainotti et al. 2022a). To determine the k parameter, one has to compute a grid of values for k and find the one that corresponds to the absence of correlation between the corrected quantity and the redshift. Therefore, the Kendall's τ coefficient is perfect for this task. Namely, we are looking for such a k for which $\tau = 0$, where, following the EP method, we define τ as:

$$\tau = \frac{\sum_i (\mathcal{R}_i - \mathcal{E}_i)}{\sqrt{\sum_i \mathcal{V}_i}}. \quad (4)$$

In this formula, for each redshift z_i in our sample, we compute the number of data points in a rectangular built intersecting the limiting luminosity $L_{\text{lim},i}$ (i.e., the lowest possible luminosity observed at a given redshift computed with the assumed limiting flux from $L_{\text{lim},i} = F_{\text{lim}} \times 4\pi d_i^2(z_i)$) and the redshift z_i itself. The associated set for z_i contains all QSOs verifying $L_{z_j} \geq L_{\text{min},i}$ and $z_j \leq z_i$, where j and i refer to objects of the associated set and the complete QSO sample, respectively. The rank \mathcal{R}_i of the data point y_i with luminosity L_i at redshift z_i is computed as the number of these data points in the corresponding associated set. Then, we subtract from the rank of each data point its expectation value corresponding to a distribution with no correlation: $\mathcal{E}_i = \frac{1}{2}(i+1)$. After summing the obtained differences, the correlation is removed when the sum is 0 (i.e., $\tau = 0$). To make this concept clearer, we present the visualization of the computation of the rank \mathcal{R}_i in the above-described rectangle in Figure 2, where the case of the X-ray luminosity is shown as an example. In Figure 2 the assumed limiting flux is $F_{\text{lim}} = 6 \times 10^{-33} \text{ erg s}^{-1} \text{ cm}^{-2} \text{ Hz}^{-1}$ (see Dainotti et al. 2022a) and in our computation, we discard

the data points that are below the value of the corresponding limiting luminosity (purple curve). This figure was obtained for demonstrative purposes under the assumption of a flat Λ CDM model with $\Omega_M = 0.3$. For completeness, we have to consider the normalization for the variance $\mathcal{V}_i = \frac{1}{12}(i^2 + 1)$. To this end, we compute τ by dividing the above-described sum by the sum of variances for each data point. To find the 1σ uncertainty on the investigated k parameter, we compute the k values corresponding to $\tau = 1$ and $\tau = -1$.

This method has already been successfully applied in the literature to many probes, including QSOs. In particular, using the same QSO sample as the one used in this work, Dainotti et al. (2022a) tested two different functional forms of $\xi(z)$ obtaining numerically compatible results. Assuming $\xi(z) = (1+z)^k$, the authors obtained $L'_X = L_X / (1+z)^{3.36 \pm 0.07}$ and $L'_{\text{UV}} = L_{\text{UV}} / (1+z)^{4.36 \pm 0.08}$, with $F_{\text{lim}} = 4.5 \times 10^{-29} \text{ erg s}^{-1} \text{ cm}^{-2} \text{ Hz}^{-1}$ for UV and $F_{\text{lim}} = 6 \times 10^{-33} \text{ erg s}^{-1} \text{ cm}^{-2} \text{ Hz}^{-1}$ for X-rays. These choices are legitimated by the authors showing that the evolutionary coefficient k depends only weakly on these assumptions: even spanning over 1 order of magnitude in F_{lim} both in UV and X-rays, the evolutionary coefficient's results remain compatible within 2σ . This was already proved in Dainotti et al. (2021c) for several sample sizes of GRBs.

As can be seen Figure 1, the application of the above-defined correction removes the dependence of the RL relation on redshift, and additionally, once corrected, the data points are evenly dispersed in redshift. Indeed, in the case without correction (left panel), the redshift increases with higher luminosities, while, once the relation is corrected for evolution (right panel), this trend completely disappears and redshifts are blended over the whole range of luminosities.

It has to be pinpointed here that the execution of such a method is possible only with an assumed cosmology, required by the computation of luminosities; thus, this technique cannot be straightforwardly applied in cosmological computations. Such a calculation of cosmological parameters would be indeed affected by the so-called circularity problem. To overcome this issue, we repeat the same procedure for a grid of cosmological parameters that fall in reasonable physical ranges of values, and we study how the k parameter behaves with cosmology. Thus, when applying this correction in the MCMC method for obtaining the values of cosmological parameters such as Ω_M , Ω_k , H_0 , and w , we consider $k = k(\Omega_M)$, $k = k(\Omega_k)$, $k = k(\Omega_M, \Omega_k)$, $k = k(\Omega_M, H_0)$, $k = k(w)$, or $k = k(\Omega_M, w)$ according to the free parameters of the model considered. Indeed, we here remind the reader that k does not depend on H_0 , since this parameter is responsible only for a scaling of the luminosity's value and does not change the correlation, as shown in Dainotti et al. (2022a), so we do not have to consider also $k = k(H_0)$. In our computations, the numerical functions $k = k(\Omega_M)$, $k = k(\Omega_k)$, and $k = k(w)$ are always created with a cubic-spline method, while $k = k(\Omega_M, \Omega_k)$ and $k = k(\Omega_M, w)$ are created with a ‘‘quintic’’ type of interpolation. Since cosmological parameters usually depend on each other and have to be fitted simultaneously in the MCMC method, we compute two maps that show how k changes in the parameter spaces $\{\Omega_M, \Omega_k\}$ and $\{\Omega_M, w\}$, which covers all cases studied in our cosmological computations (see Figure 3). We comment on the results of these investigations in Section 5.1.

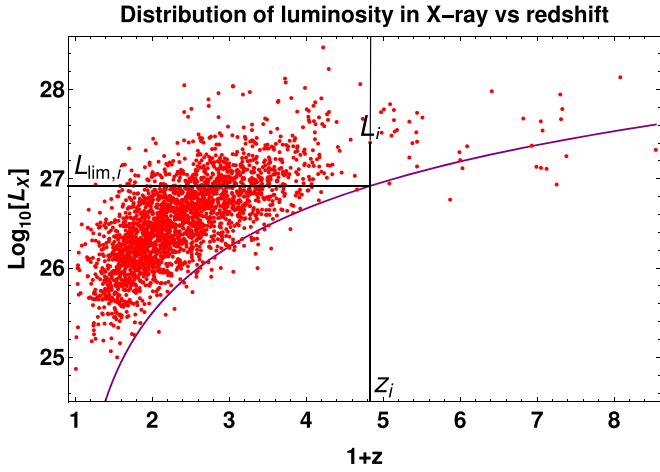


Figure 2. X-ray luminosity (in logarithmic units) vs. $(1+z)$. The solid purple curve shows the truncation due to the flux limit, which is here assumed to be $F_{\text{lim}} = 6 \times 10^{-33} \text{ erg s}^{-1} \text{ cm}^{-2} \text{ Hz}^{-1}$ (Dainotti et al. 2022a). The rank \mathcal{R}_i of the point of luminosity L_i at redshift z_i is the number of points in the rectangle within black lines, with points under the purple curve being discarded. This figure is computed under the assumption of a flat Λ CDM model with $\Omega_M = 0.3$.

3.3. Calibration Methodology

Many attempts have been made in the literature to improve cosmological constraints by applying the so-called calibration method. This approach is based on anchoring a probe to another one that presents an overlapping redshift range and has measured distances. This procedure is commonly applied, for example, to calibrate SNe Ia with the distances of Cepheids measured through their pulsation period–luminosity relation (see, e.g., Sandage et al. 1996; Riess et al. 2009). This has led to the so-called cosmic distance ladder to measure distances in the universe. At redshifts higher than the ones explored by SNe Ia, the most commonly used technique assumes that high- z cosmological probes follow the same cosmology as SNe Ia in their common redshift range. Thus, the subsample composed only of sources observed up to the maximum redshift of SNe Ia is fitted under the assumption of a cosmological model with parameter values based on the computations with SNe Ia. The parameters of the correlation are then fixed to the values obtained assuming the cosmology obtained by SNe Ia in that particular overlapping region. This approach is the one we follow in this work to calibrate QSOs. As the maximum redshift of our SNe Ia data set is $z = 2.26$, we create our calibrating subsample composed of 2066 QSOs (out of the initial 2421 sources) and fit the RL relation on this subsample combined with SNe Ia. The results of the MCMC fitting without correcting for evolution in redshift of luminosities are as follows: $g = 0.648 \pm 0.009$, $b = 6.817 \pm 0.265$, and $sv = 0.234 \pm 0.004$. Once the correction for evolution is applied, we obtain: $g' = 0.591 \pm 0.013$, $b' = 8.278 \pm 0.0362$, $sv' = 0.231 \pm 0.004$, where the ' symbol stands for the same parameters as before but once the correction is applied.

4. The Cosmological Models

In this work, we investigate three cosmological models, which are the most commonly studied in recent analyses. In both cases, the considered cosmological components are: DE (indicated by the subscript Λ), nonrelativistic matter (M),

including both baryons (b) and CDM ($_{\text{CDM}}$), and the relativistic component (r), composed of radiation (γ) and neutrinos (ν). The last one makes a negligible contribution to the late universe (in which $\Omega_r = \Omega_\gamma + \Omega_\nu = 9 \times 10^{-5}$); thus, we set the current relativistic density parameter Ω_r equal to 0 in our computation.

In the first case, we consider a universe with a potential nonzero curvature of spacetime, in which all parameters are connected via the relation $1 = \Omega_r + \Omega_M + \Omega_\Lambda + \Omega_k$. Within this model, the luminosity distance d_l is given by:

$$d_l = (1+z) \frac{c}{H_0} \begin{cases} \frac{1}{\sqrt{|\Omega_k|}} \sin\left(\sqrt{|\Omega_k|} \int_0^z \frac{d\zeta}{E(\zeta)}\right) & \text{if } \Omega_k < 0, \\ \int_0^z \frac{d\zeta}{E(\zeta)} & \text{if } \Omega_k = 0, \\ \frac{1}{\sqrt{\Omega_k}} \sinh\left(\sqrt{\Omega_k} \int_0^z \frac{d\zeta}{E(\zeta)}\right) & \text{if } \Omega_k > 0, \end{cases} \quad (5)$$

where $E(\zeta)$ stands for the dimensionless Hubble parameter defined as

$$E(\zeta) = \frac{H(\zeta)}{H_0} = \sqrt{\Omega_r(1+\zeta)^4 + \Omega_M(1+\zeta)^3 + \Omega_k(1+\zeta)^2 + \Omega_\Lambda}. \quad (6)$$

$\Omega_k = 0$ corresponds to a flat spacetime, and we refer to the model with this fixed value as the flat Λ CDM model, while the model with any possible value of Ω_k is referred to as the nonflat Λ CDM model.

The other model investigated in this work is the most natural extension of the Λ CDM scenario. Indeed, we consider an equation of state of DE $w = P_\Lambda/\rho_\Lambda$, where P_Λ and ρ_Λ are the pressure and energy density of DE, respectively, which can assume any constant value. The case with $w = -1$ corresponds to the Λ CDM model. In this model, Equation (5) changes only in the form of the $E(\zeta)$ function, which becomes

$$E_w(\zeta) = \sqrt{\Omega_r(1+\zeta)^4 + \Omega_M(1+\zeta)^3 + \Omega_k(1+\zeta)^2 + \Omega_\Lambda(1+\zeta)^{3(1+w)}}. \quad (7)$$

In this case, we assume a flat universe fixing $\Omega_k = 0$ and, as a consequence, $\Omega_\Lambda = 1 - \Omega_M - \Omega_r$. This assumption is consistent with the most recent cosmological observations on the CMB (Planck Collaboration et al. 2020) and other recent studies (e.g., Alam et al. 2021; Gonzalez et al. 2021), where nonflat universes are consistent with zero curvature.

4.1. Assumptions on Cosmological Parameters

It is worth mentioning some of the assumptions we use in our cosmological analyses. First of all, in all models, we use flat uniform priors on the free parameters as follows: $0 \leq \Omega_M \leq 1$, $60 \leq H_0 \leq 80$, $-2.5 \leq w \leq -0.34$, and $-0.9 \leq \Omega_k \leq 0.6$. The limits on Ω_k have been increased to obtain convergence in all cases studied. The upper limit on w is imposed following the second Friedmann's equation, according to which we need $w(z) < -1/3$ to explain the present accelerated expansion of the universe (Riess et al. 1998;

Perlmutter et al. 1999) as a DE dominant effect. In addition to these priors, we do not look for solutions to the values of cosmological parameters in the whole parameter space, as there are regions that lead to nonphysical or nonreasonable solutions. Thus, in our analyses, we discard the part of the $\{\Omega_M, \Omega_k\}$ parameter space that leads to the “no Big Bang” solutions, which do not admit an initial singularity. Following Carroll et al. (1992), the region that admits physical solutions with an initial singularity in a Λ CDM model corresponds to:

$$\Omega_k \geq \begin{cases} 1 - \Omega_M - 4 \Omega_M \cosh^3 \left[\frac{1}{3} \operatorname{arccosh} \left(\frac{1 - \Omega_M}{\Omega_M} \right) \right] & \Omega_M \leq \frac{1}{2}, \\ 1 - \Omega_M - 4 \Omega_M \cos^3 \left[\frac{1}{3} \arccos \left(\frac{1 - \Omega_M}{\Omega_M} \right) \right] & \Omega_M > \frac{1}{2}. \end{cases} \quad (8)$$

Part of the discarded region can be seen in both panels of the upper row of Figure 3 under the dashed black line.

Furthermore one can consider only the region of Ω_M, w space that does not lead to present values of the Hubble constant higher than its value in the past. This would allow only for the case of $\frac{dH(z)}{dz}|_{z=0} \geq 0$, which satisfies the null energy condition (Visser & Barcelo 2000). Taking the derivative of Equation (7) and substituting $z=0$, one can obtain the following criteria:

$$w \geq \frac{1}{\Omega_M - 1}. \quad (9)$$

The border set up by this condition is shown in both panels of the bottom row in Figure 3 with a thick white line. The depicted region can be a test of violation of the null energy condition regarding the present discussion about its viability.

5. Results

In this section, we present and comment on the results of our analyses. Section 5.1 is focused on how the correction for evolution in redshift of luminosities is impacted by cosmological parameters (see Figures 3 and 4). Sections 5.2–5.4 show the cosmological constraints obtained in all three models studied in this work considering all of the data sets and approaches used. Tables 1 and 2 report, for each case studied, the mean values of free cosmological parameters with their corresponding 1σ error. Figures 6–9 show the corresponding corner plots obtained in the cosmological computations.

5.1. Impact of Cosmology on Correction for Evolution

All of the cases considered in this work present a smooth dependence of k on cosmological parameters (i.e., there are no bumps or discontinuities in computations) for both k_{L_X} and $k_{L_{UV}}$. The upper row of Figure 4 shows how k depends on the parameter determining the curvature of the universe Ω_k with fixed $\Omega_M=0.3$ for both UV (left panel) and X-ray (right panel) cases. In both panels, the computed dependence has a similar trend, with values of k that do not vary much for values of Ω_k close to $\Omega_k=0$ (the ones expected from the most recent observations and studies). For a matter of a pure, more theoretical discussion on how close these solutions are to the nonphysical regions, also showing peculiar behavior in terms of the evolution, we can observe the following features: at the negative values far from $\Omega_k=0$, a rapid decrease of k values is present, and k becomes incompatible within 3σ with the value

computed for $\Omega_k=0$ at $\Omega_k \sim -0.7$ for both quantities considered. In all of the panels, we mark with a thick, black line the values of k_{L_X} and $k_{L_{UV}}$ computed for $\Omega_M=0.3$, $\Omega_k=0$, and $w=-1$ together with 1σ , 2σ , and 3σ error bars marked with red, orange, and green dashed lines, respectively. We also computed values of the k -parameters for values of Ω_k close to 1, and we observe that these values do not change significantly from the highest value shown on the plot ($\Omega_k=0.2$). Thus, as we do not exceed this region in our computations, we show on the plot only a range of Ω_k between -0.9 and 0.2 . The upper row of Figure 3 shows instead the results of a more general approach, in which we compute the value of k over a grid of values of both Ω_M and Ω_k , as described in Section 3.2. The variation of both k_{L_X} and $k_{L_{UV}}$ with these cosmological parameters is very similar. Unsurprisingly, the most significant evolution of the luminosities appears in the region close to the point $\{\Omega_M=0, \Omega_k=0\}$, because in such a universe $E(\zeta)$ would become $E(\zeta)=1$, and it would result in a quadratic function of the distance luminosity with redshift, which would lead to still quite a dispersed but power-of-four relation of the luminosity with the redshift. Values of k close to the restricted region marked with the black dashed line rapidly decrease with distance from the origin of axes. We can conclude that, in reasonable regions of this parameter space (i.e., near $\{\Omega_M=0.3, \Omega_k=0\}$), the values of k are compatible with the ones obtained for $\Omega_k=0$ and $\Omega_M=0.3$. As is visible from the plots, we discard a part of the $\{\Omega_M, \Omega_k\}$ space bigger than the region defined by Equation (8). Indeed, the rapid decrease of k values close to this region affects the precision of the interpolation method that we use to compute the function $k(\Omega_M, \Omega_k)$, which we then use for our cosmological computations. Nevertheless, we must note that this discarded region does not impact our analysis, as our results do not fall in this cutoff region in any of the cases.

Results of the investigation of the dependence of k on the w -parameter fixing $\Omega_M=0.3$ are shown in the bottom row of Figure 4 for both the UV (left panel) and X-ray cases (right panel). Within the whole range of w values explored, k values are compatible with the value obtained for $w=-1$ within less than 2σ . Thus, we do not expect a significant difference in cosmological results between the computation of w with fixed correction for evolution and the one with $k=k(w)$. If we look at the more general investigation in the parameter space of both Ω_M and w presented in the bottom row of Figure 3, we see that, as in the previous case, the variation of both k_{L_X} and $k_{L_{UV}}$ with the cosmological parameters presents very similar features, and in reasonable regions of this parameter space $\{\Omega_M, w\}$ (i.e., near $\{\Omega_M=0.3, w=-1\}$), the values of k are compatible with those obtained for $\Omega_M=0.3$ and $w=-1$, while k 's values vary more significantly in exotic regions of this space. Due to high dispersion of the RL relation, our analyses still cover a large range of the cosmological parameters. Thus, the change of evolutionary parameter, k , with cosmology could still be significant in some computations. For example, when using $k=k(\Omega_M, w)$ for the joint sample of SNe Ia and QSOs, the 3σ contours in the $\{\Omega_M, w\}$ space extend from $\Omega_M=0.2$ and $w=-0.8$ to $\Omega_M=0.5$ and $w=-1.6$ (see plot (i) in Figure 9). In this case, we find that the values of $k_{L_{UV}}$ vary from 4.13 ± 0.08 (for $\Omega_M=0.5$ and $w=-1.6$) up to 4.47 ± 0.08 (for $\Omega_M=0.2$ and $w=-0.8$). Thus, the values of k result to be compatible with each other within 3σ , while k_{L_X} varies from 3.13 ± 0.06 (for $\Omega_M=0.5$ and $w=-1.6$) up to 3.48 ± 0.06

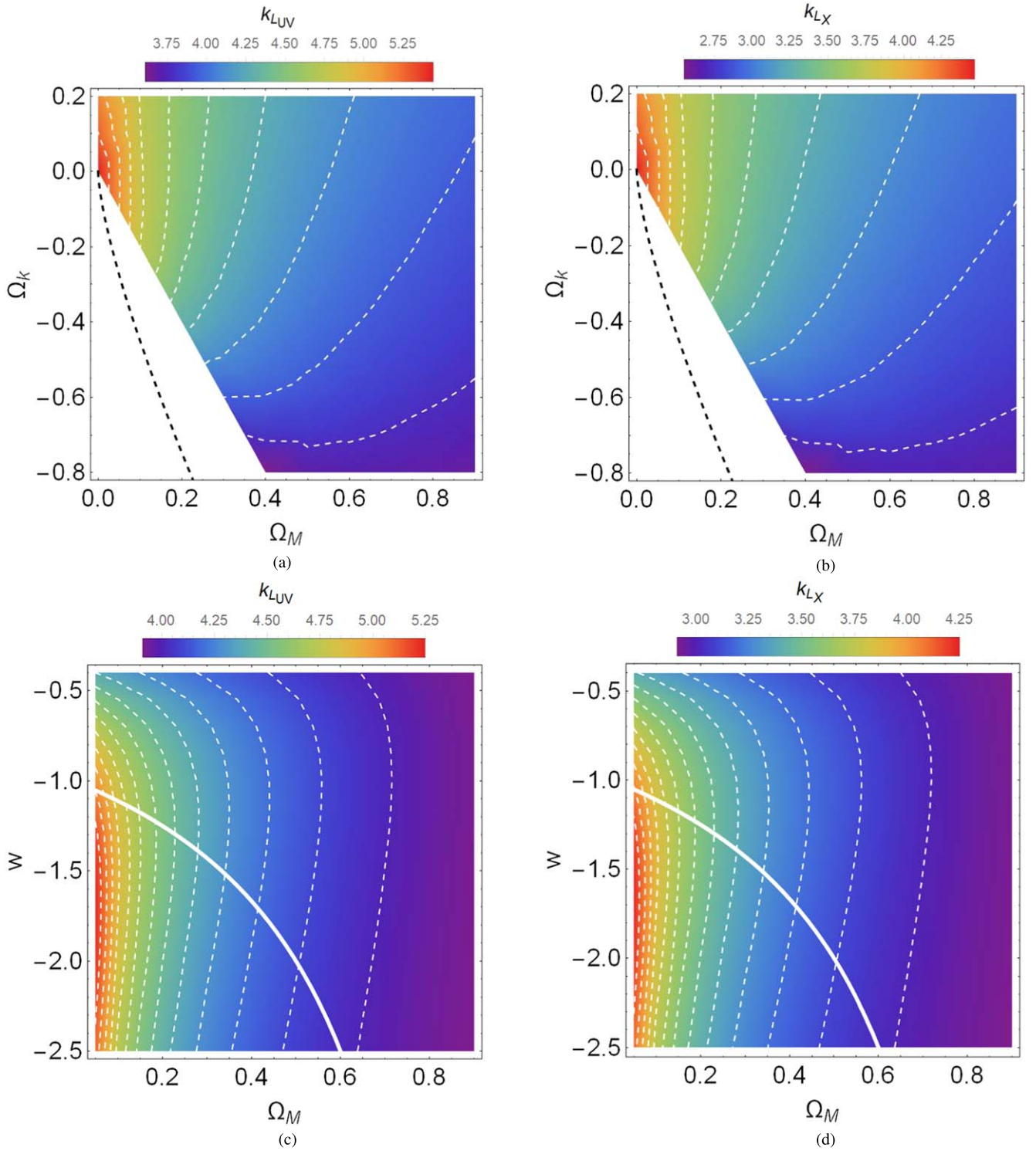


Figure 3. Behavior of the k parameter in the parameter spaces $\{\Omega_M, \Omega_k\}$ (panels (a) and (b)) and $\{\Omega_M, w\}$ (panels (c) and (d)) for both UV (left panels) and X-rays (right panels). (a) Behavior of the k parameter in the parameter space $\{\Omega_M, \Omega_k\}$ for UV. The dashed black line shows the “no Big Bang” constraint (see Section 4.1 and Equation (8)). (b) Behavior of the k parameter in the parameter space $\{\Omega_M, \Omega_k\}$ for X-rays. The dashed black line shows the “no Big Bang” constraint (see Section 4.1 and Equation (8)). (c) The behavior of the k parameter in the parameter space $\{\Omega_M, w\}$ for UV. The region under the thick white line corresponds to the scenario of $H'(z)|_{z=0} \leq 0$, while the region above the following line corresponds to $H'(z)|_{z=0} > 0$. (d) The behavior of the k parameter in the parameter space $\{\Omega_M, w\}$ for X-rays. The region under the thick white line corresponds to the scenario of $H'(z)|_{z=0} \leq 0$, while the region above the following line corresponds to $H'(z)|_{z=0} > 0$.

(for $\Omega_M = 0.2$ and $w = -0.8$), being compatible with each other within 4σ . The explored range of k values in the MCMC fitting becomes even wider when we consider the case of QSOs alone, both calibrated and noncalibrated. Thus, the variation of k with cosmology is often not negligible.

In the approach presented in this article, we also compute, in all considered cases, the error on k values as a function of cosmology. In reasonable ranges, we always observe very small variations of the error with cosmology. As is visible in the upper row of Figure 4, the error on k for $\Omega_k < -0.8$ is

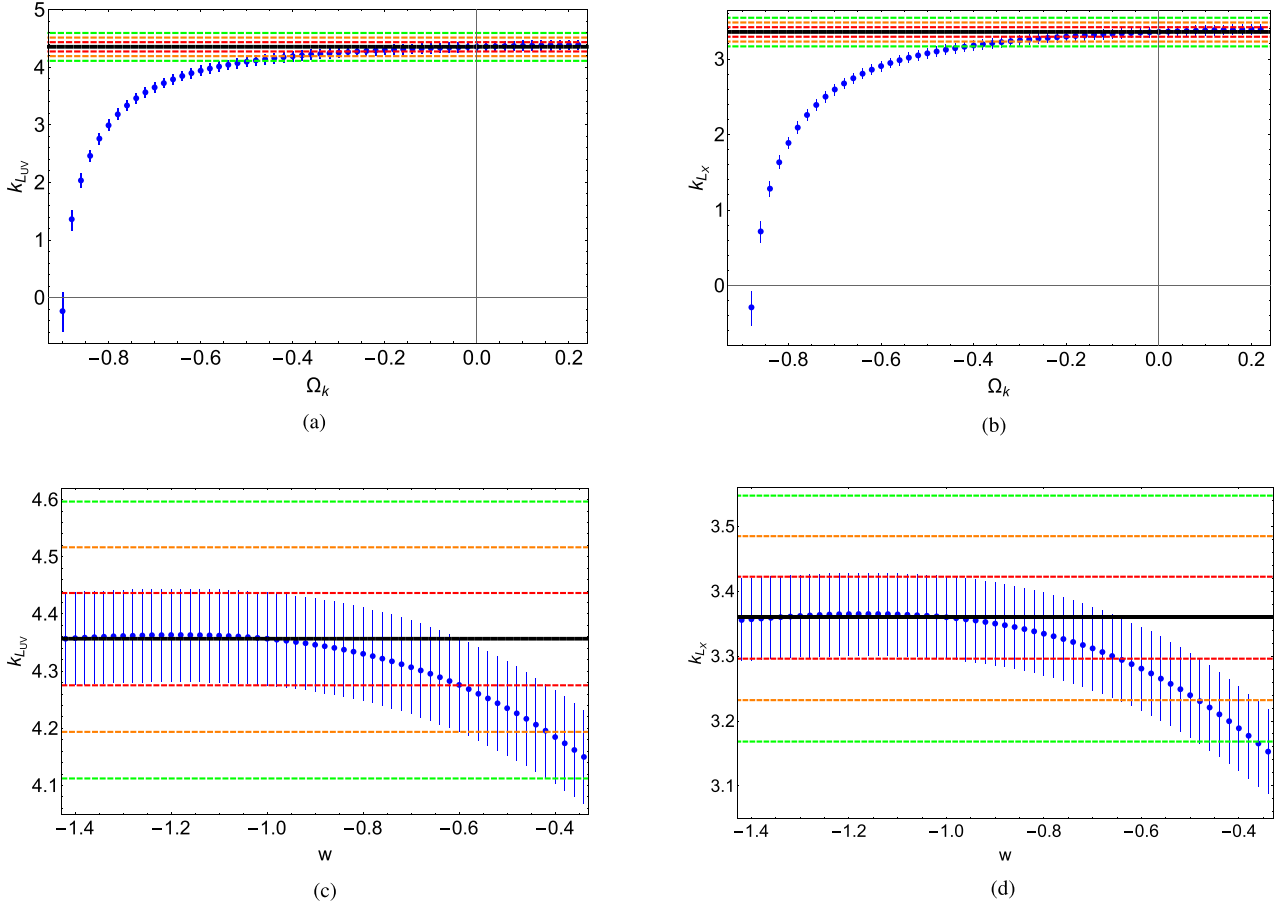


Figure 4. We mark with a thick, black line the values of k_{LX} and k_{LUV} computed for the $\Omega_M = 0.3$, $\Omega_k = 0$, and $w = -1$ together with 1σ , 2σ , and 3σ error bars marked with red, orange, and green dashed lines, respectively. (a) Behavior of k -parameter for the correction of L_{UV} in relation to Ω_k for a nonflat Λ CDM model with $\Omega_M = 0.3$. (b) Behavior of k -parameter for the correction of L_X in relation to Ω_k for a nonflat Λ CDM model with $\Omega_M = 0.3$. (c) Behavior of k -parameter for L_{UV} in relation to w for a flat w CDM model with $\Omega_M = 0.3$. (d) Behavior of k -parameter for L_X in relation to w for a flat w CDM model with $\Omega_M = 0.3$.

about twice the size of that for $\Omega_k = 0$; but for values of $\Omega_k > -0.55$, the errors are $<8\%$ larger than those for $\Omega_k = 0$ for both $k_{LX}(\Omega_k)$ and $k_{LUV}(\Omega_k)$. Concerning the error $\Delta_k(w)$, we do not observe variations of the errors larger than 4% across the entire considered region for both $k_{LX}(w)$ and $k_{LUV}(w)$ (see the bottom row of Figure 4). For $\Delta_k(\Omega_M, \Omega_k)$, we always observe variations $<7\%$ for every computed point for both $k_{LX}(\Omega_M, \Omega_k)$ and $k_{LUV}(\Omega_M, \Omega_k)$. The same result is obtained for the errors $\Delta_k(\Omega_M, w)$, for both $k_{LX}(\Omega_M, w)$ and $k_{LUV}(\Omega_M, w)$. Thus, in future analyses, the evolution of the errors on the k -parameter with cosmology could be possibly neglected.

5.2. Results on the Flat Λ CDM Model

5.2.1. Calibrated QSOs Alone

Assuming a flat Λ CDM model, the case with QSOs alone calibrated with SNe Ia and without any correction for evolution favors high values of Ω_M , even if compatible in 3σ with $\Omega_M = 0.3$, when H_0 is fixed, and high values of H_0 when Ω_M is fixed, while, when both parameters are free, we do not obtain convergence on the Ω_M parameter, which tends to have very high values even outside our uniform prior bound. Including a fixed correction for the evolution instead, Ω_M always goes to lower values, both for fixed and free H_0 ($\Omega_M = 0.251 \pm 0.054$ and $\Omega_M = 0.167 \pm 0.062$, respectively), while H_0 ranges from

67.55–72.09 $\text{km s}^{-1} \text{Mpc}^{-1}$ in 1σ when Ω_M is fixed, corresponding to intermediate values between the one measured from SNe Ia ($H_0 = 74.03 \pm 1.42 \text{ km s}^{-1} \text{Mpc}^{-1}$) and the one obtained from the Planck data on the CMB under the assumption of the same cosmological model ($H_0 = 67.4 \pm 0.5 \text{ km s}^{-1} \text{Mpc}^{-1}$). The case with both parameters free does not converge for either of the two parameters, leading to too low Ω_M values ($\Omega_M = 0.167 \pm 0.062$), compatible within 3σ with the theoretical De Sitter universe in which $\Omega_M = 0$, and too high H_0 values ($H_0 = 76.40 \pm 3.33 \text{ km s}^{-1} \text{Mpc}^{-1}$). Taking into account the variation of the correction for evolution together with the cosmological parameter Ω_M , Ω_M becomes consistent with $\Omega_M = 0.3$, when H_0 is fixed, also due to large uncertainties, but Ω_M does not converge when H_0 is free to vary, going to the upper limit of our uniform prior. In this case, H_0 is compatible within 1σ with the value from the CMB.

5.2.2. Noncalibrated QSOs together with SNe Ia

When combining noncalibrated QSOs with SNe Ia, we do not deal with convergence issues in any of the cases. Specifically, without accounting for the correction for evolution, we find Ω_M close to 0.3 (in 1σ and 2σ when H_0 is fixed and free, respectively) and H_0 close to 70 (in 1σ and 2σ when Ω_M is fixed and free, respectively). When accounting for a fixed correction for evolution, we still have Ω_M close to 0.3 even if in

Table 1
Cosmological Results Obtained for All Considered Cases

Only QSOs Calibrated on SNe Ia				Combination of SNe Ia with QSOs without Calibration			
Results without Correction for Evolution							
Ω_M	H_0	w	Ω_k	Ω_M	H_0	w	Ω_k
0.443 ± 0.054	70	-1	0	0.305 ± 0.008	70	-1	0
0.3	73.76 ± 2.18	-1	0	0.3	69.97 ± 0.14	-1	0
0.663 ± 0.108	62.77 ± 2.52	-1	0	0.338 ± 0.022	69.44 ± 0.32	-1	0
0.3	70	-0.696 ± 0.132	0	0.3	70	-1.003 ± 0.019	0
0.3	70	-1	-0.531 ± 0.275	0.3	70	-1	-0.01 ± 0.018
0.522 ± 0.052	70	-1.966 ± 0.395	0	0.462 ± 0.034	70	-1.552 ± 0.166	0
0.517 ± 0.06	70	-1	-0.740 ± 0.106	0.656 ± 0.048	70	-1	-0.762 ± 0.101
Results with Fixed Correction for Evolution							
Ω_M	H_0	w	Ω_k	Ω_M	H_0	w	Ω_k
0.251 ± 0.040	70	-1	0	0.291 ± 0.008	70	-1	0
0.3	69.82 ± 2.27	-1	0	0.3	69.99 ± 0.14	-1	0
0.167 ± 0.062	76.40 ± 3.33	-1	0	0.251 ± 0.02	70.72 ± 0.34	-1	0
0.3	70	-1.113 ± 0.182	0	0.3	70	-1.006 ± 0.018	0
0.3	70	-1	0.01 ± 0.122	0.3	70	-1	0. ± 0.018
0.151 ± 0.099	70	-0.765 ± 0.267	0	0.059 ± 0.038	70	-0.662 ± 0.041	0
0.24 ± 0.05	70	-1	0.076 ± 0.104	0.118 ± 0.032	70	-1	0.377 ± 0.069
Results with Correction for Evolution as Function of Cosmology							
Ω_M	H_0	w	Ω_k	Ω_M	H_0	w	Ω_k
0.382 ± 0.178	70	-1	0	0.299 ± 0.008	70	-1	0
0.543 ± 0.251	67.50 ± 2.80	-1	0	0.3 ± 0.022	69.99 ± 0.35	-1	0
0.3	70	-1.074 ± 0.205	0	0.3	70	-1.005 ± 0.019	0
0.3	70	-1	-0.041 ± 0.102	0.3	70	-1	-0.006 ± 0.018
0.546 ± 0.172	70	-1.591 ± 0.500	0	0.358 ± 0.054	70	-1.168 ± 0.156	0
0.591 ± 0.217	70	-1	-0.235 ± 0.191	0.415 ± 0.063	70	-1	-0.250 ± 0.134

Note. In the upper part of the table, we show the results without the correction for evolution. In the middle part, we show the results obtained with fixed evolution, and at the bottom, we show the results obtained with correction for evolution as a function of cosmology. Errors reported in the table correspond to 1σ uncertainties. Bold values represent the values fixed for Ω_M and H_0 in the corresponding cosmological analysis.

Table 2

Cosmological Results Obtained with only the QSO Sample without Calibration

Results Obtained with QSOs Alone without Calibration	Ω_M
Results without correction for evolution	0.934 ± 0.059
Results with fixed correction for evolution	0.067 ± 0.017
Results with correction for evolution as a function of Ω_M	0.500 ± 0.210

Note. We show the results without the correction for evolution, with fixed correction for evolution, and with correction for evolution as a function of Ω_M . Errors reported in the table correspond to 1σ uncertainties. In this computation we fix the parameters as $H_0 = 70 \text{ km s}^{-1} \text{ Mpc}^{-1}$, $\Omega_k = 0$, and $w = -1$.

2σ and 3σ when H_0 is fixed and free, respectively, and H_0 close to 70, in 1σ and 3σ when Ω_M is fixed and free, respectively. Letting the evolution vary together with the cosmological

parameter (i.e., $k(\Omega_m)$), we obtain Ω_M and H_0 always compatible within 1σ with 0.3 and 70, respectively. Indeed, we here remind the reader that k does not depend on H_0 , as was already stressed, so we do not have to, again, study the case in which only H_0 is free.

Since in these cases we are not calibrating QSOs with SNe Ia, we also fit g , b , and sv contemporaneously with the cosmological parameters. Without evolution, we always obtain $g = 0.66 \pm 0.01$ independently of the number of free parameters, in which b is always compatible within 1σ with a central value of $b = 6.33$, and $sv = 0.230 \pm 0.004$ in all cases. When we account for the correction for evolution, both fixed or as a function of cosmological parameters, we obtain $g = 0.59 \pm 0.01$, in which b is always compatible within 1σ with a central value of $b = 8.24$, and $sv = 0.225 \pm 0.003$ in all

cases. We note that the correction for evolution reduces the intrinsic dispersion by 2.2%, making the RL relation tighter.

5.2.3. Noncalibrated QSOs Alone

Only in this case of a flat Λ CDM model do we also consider the data set composed of QSOs alone noncalibrated on SNe Ia to investigate how this sample can impact the determination of the Ω_M parameter in the cosmological analysis. These results are shown in Table 2 and Figure 7, where H_0 is fixed to $H_0 = 70 \text{ km s}^{-1} \text{ Mpc}^{-1}$. If we do not consider the correction for the evolution, Ω_M is not constrained and hits the upper limit $\Omega_M = 1$ in the range of uniform priors. Once accounting for a fixed correction for the evolution instead, we obtain closed contours on this parameter, but with values shifted to very small values $\Omega_M = 0.067 \pm 0.017$, although not compatible with $\Omega_M = 0$ within 3σ . Unsurprisingly, the case with the correction $k = k(\Omega_M)$ allows us to overcome the convergence issue and the nonphysical behavior with Ω_M close to 0, leading to $\Omega_M = 0.500 \pm 0.201$, which is compatible within 1σ with $\Omega_M = 0.3$. Concerning the values of the parameters of the RL relation, we obtain consistency with the ones from noncalibrated QSOs combined with SNe Ia, as well as a similar reduction in the intrinsic dispersion when accounting for the correction for the evolution. Concerning this, we have also tried to compute other cosmological parameters such as H_0 , Ω_k , and w for the sample composed of QSOs alone without calibration, but we have not obtained closed contours in any of these cases; thus, we do not show these results here. This can be ascribed to the fact that the RL relation, even after the correction for evolution, still retains an intrinsic scatter. Thus, noncalibrated QSOs alone are too weak to constrain parameters of more complex models. Our results show a path in which further investigations of the properties of this probe could lead to tighter, more reliable results.

5.3. Results on the Nonflat Λ CDM Model

5.3.1. Calibrated QSOs Alone

When allowing for $\Omega_k \neq 0$, QSOs alone calibrated with SNe Ia point toward negative values of Ω_k , if we do not correct for luminosity evolution in redshift. More precisely, $\Omega_k = -0.531 \pm 0.275$ when Ω_M is fixed, while, when both are free parameters of the fit, Ω_M tends to 0.52, but Ω_k does not converge due to too low values in our range of uniform prior. Very interestingly, when we correct for a fixed evolution, convergence is reached for both Ω_k and Ω_M left free to vary (however, with large uncertainties), while Ω_M shifts toward 0.3 and Ω_k toward 0. Instead, when Ω_k is the only free parameter of the fit, it is not constrained, as happens when also accounting for a correction that varies with Ω_k . This can be ascribed to the fact that QSOs are more sensitive to the value of Ω_M , which is better determined by probes at intermediate redshifts, rather than the value of Ω_k , which is instead constrained at very high redshifts as that of CMB; thus, when Ω_M is also free, QSOs can constrain Ω_M and, as a consequence of their degeneracy, also Ω_k . Varying both parameters and taking into account a correction for evolution that varies together with these parameters does not constrain Ω_M , which tends to have values close to $\Omega_M = 1$.

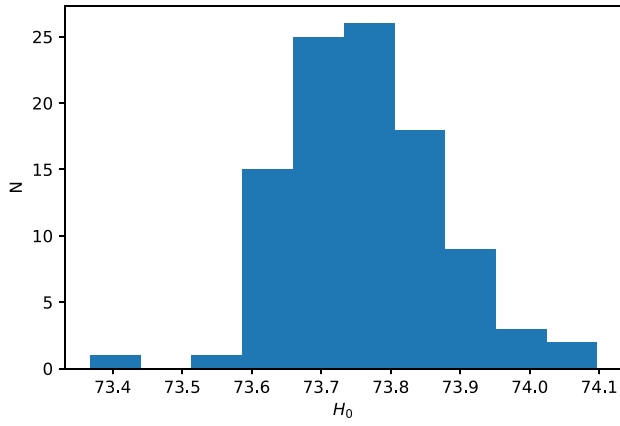
5.3.2. Noncalibrated QSOs together with SNe Ia

In the case of noncalibrated QSOs combined with SNe Ia, Ω_k is always compatible with $\Omega_k = 0$ within 1σ when Ω_M is fixed to 0.3 (as expected for a flat universe), both with and without the correction for the evolution, while, when Ω_M is also free, it tends to negative values (i.e., $\Omega_k = -0.762 \pm 0.101$) if we do not correct for evolution, and to positive values (i.e., $\Omega_k = 0.377 \pm 0.069$) when considering a fixed correction. In these two cases, Ω_M is shifted to high and low values, respectively. When accounting for the correction with $k(\Omega_M, \Omega_k)$, we observe an intermediate behavior: $\Omega_M = 0.415 \pm 0.063$, within 2σ from $\Omega_M = 0.3$, and $\Omega_k = -0.250 \pm 0.134$, within 3σ from a zero curvature.

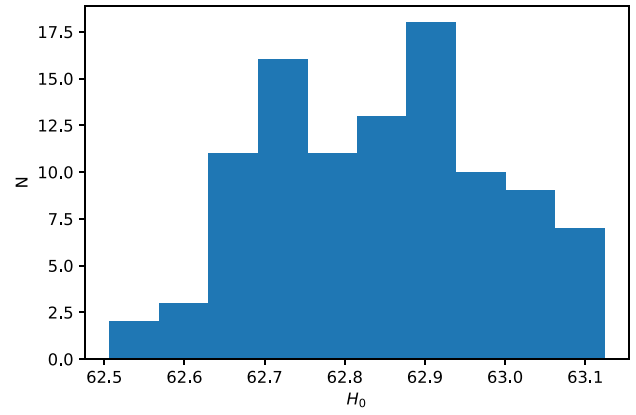
Concerning the free parameters of the RL relation, the results are the same as those obtained for the flat Λ CDM model, showing that the values of these parameters do not depend on the curvature of the universe. In addition, comparing the values of g and b obtained when only Ω_k is the free parameter and when both Ω_M and Ω_k are free parameters, we note that there are slight discrepancies ($\sim 2\sigma$) in the case without evolution, which are completely removed once the evolution is taken into account. This shows that the correction for the luminosity evolution makes the parameters of the RL relation compatible within 1σ , comparing the cases with different numbers of free parameters. Many computations involving QSOs through the literature concerning the value of Ω_k show traces of its value being smaller than zero (Khadka & Ratra 2022). Our results could indicate that this behavior is due to selection bias and redshift evolution since, after this correction treated as a function of cosmology is applied, the obtained values of Ω_k become more compatible with zero. For the computations with noncalibrated QSOs together with SNe for the case without correction for evolution varying only Ω_k , we obtain $\Omega_k = -0.010 \pm 0.018$, while in the analogous case with applied correction for evolution as a function of cosmology, $\Omega_k = -0.006 \pm 0.018$. For the computations with noncalibrated QSOs together with SNe for the case without correction for evolution varying Ω_k together with Ω_M , we obtain $\Omega_k = -0.010 \pm 0.018$ and $\Omega_M = 0.656 \pm 0.048$, while in the analogous case with applied correction for evolution as a function of cosmology, $\Omega_k = -0.250 \pm 0.134$ and $\Omega_M = 0.415 \pm 0.063$. Very similar behavior can be seen in the cases with calibrated QSOs. We see here that the results after the correction for evolution as a function of cosmology is applied are much closer to the flat Λ CDM model parameters obtained with SNe alone than those without this correction. This could indicate that previous results in the literature showing values of Ω_k that are incompatible with zero were possibly driven simply by the selection bias and redshift evolution. In order to obtain clear conclusions on the flatness of the universe, more work still needs to be done. This issue could be solved in the future with a larger sample of QSOs and the addition of more high-redshift probes, like GRBs.

5.4. Results on the Flat w CDM Model

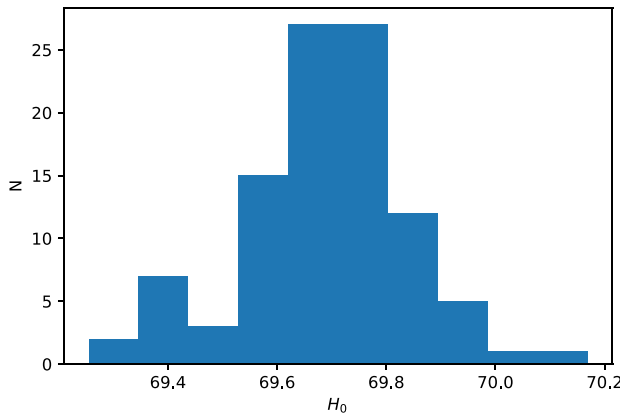
Considering the flat w CDM model, we need to distinguish between two different DE regimes in the values of the equation-of-state parameter w . Indeed, the regime $w > -1$ is referred to as a ‘‘quintessence,’’ while that with $w < -1$ as



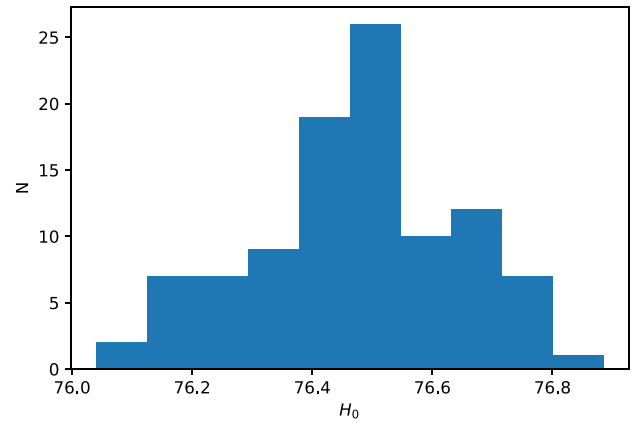
(a) Only QSOs calibrated without evolution, varying only H_0



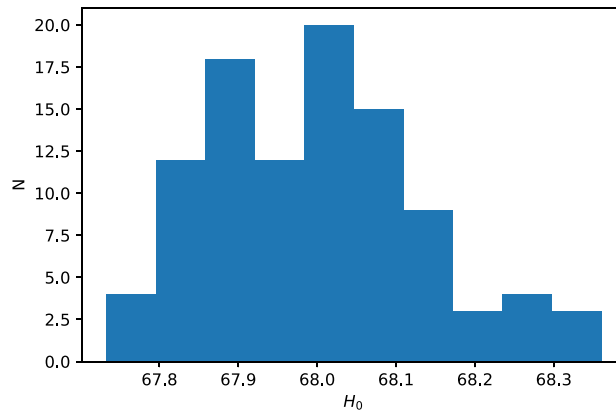
(b) Only QSOs calibrated without evolution, varying H_0 together with Ω_M



(c) Only QSOs calibrated with fixed evolution, varying only H_0



(d) Only QSOs calibrated with fixed evolution, varying H_0 together with Ω_M



(e) Only QSOs calibrated with evolution as a function of cosmology, varying H_0 together with Ω_M

Figure 5. The results of the 100 looped fits of the H_0 -parameter for all cases with calibrated QSOs. H_0 is in units of $\text{km s}^{-1} \text{Mpc}^{-1}$.

“phantom.” The phantom DE scenario predicts a final “Big Rip” for the universe in which all of the matter is ripped apart by the accelerated expansion. In relation to a region of the viability of the null energy condition given by Equation (9), none of our computations shows any trace of violation of this condition.

5.4.1. Calibrated QSOs Alone

If we consider QSOs alone calibrated with SNe Ia and we do not take into account any correction for evolution, we obtain very different results concerning the DE scenario, depending on if we did or did not fixed the parameter Ω_M . In particular, if

Table 3Comparison of Results for the H_0 -parameter Obtained in This Work with Different Approaches

Considered Case	$H_0 \left[\frac{\text{km}}{\text{Mpc} \times \text{s}} \right]$	z -score
Without calibration QSOs+SNe		
$k = k(\Omega_M)$, H_0 varied with Ω_m	69.99 ± 0.35	4.24
Fixed evolution, H_0 varied with Ω_m	70.72 ± 0.34	5.49
Fixed evolution, H_0 varied alone	69.99 ± 0.14	4.99
No evolution, H_0 varied with Ω_m	69.44 ± 0.32	3.44
No evolution, H_0 varied alone	69.97 ± 0.14	4.95
Calibrated QSOs alone		
$k = k(\Omega_M)$, H_0 varied with Ω_m	68.00 ± 2.61	0.23
Fixed evolution, H_0 varied with Ω_m	76.48 ± 3.04	2.95
Fixed evolution, H_0 varied alone	69.68 ± 2.19	1.01
No evolution, H_0 varied with Ω_m	62.84 ± 2.41	1.86
No evolution, H_0 varied alone	73.76 ± 2.18	2.84

Note. The z -score marking the compatibility of our results with the results obtained with Planck data is computed as $z_i = \frac{|H_{0,\text{CMB}} - H_{0,i}|}{\sqrt{\sigma_{\text{CMB}}^2 + \sigma_i^2}}$, where $H_{0,\text{CMB}} \pm \sigma_{\text{CMB}} = 67.4 \pm 0.5 \frac{\text{km}}{\text{Mpc} \times \text{s}}$ is the measurement of the Hubble constant with the Planck data, and $H_{0,i} \pm \sigma_i$ is one of our measurements.

$\Omega_M = 0.3$, we obtain $w \sim -0.7$, corresponding to the quintessence behavior (even if compatible within 3σ with $w = -1$). If Ω_M is a free parameter of the fit, we run into the phantom DE region with $w \sim -2$ and $\Omega_M \sim 0.5$, even if, in this case, w does not converge, going to values too negative compared to our uniform prior on this parameter. On the other hand, we observe the opposite trend when accounting for a fixed correction for evolution. In this case, indeed, the phantom regime is obtained with Ω_M fixed (but at only 1σ from a quintessence case with $w = -0.931$) and the quintessence regime (at 1σ from $w = -1$) with Ω_M as a free parameter, even if in this latter case Ω_M does not converge, hitting the barrier at $\Omega_M = 0$. When considering $k = k(w)$ with Ω_M fixed, w results are compatible with both scenarios in 1σ . When Ω_M is free to vary instead, both parameters are unconstrained.

5.4.2. Noncalibrated QSOs together with SNe Ia

When fitting jointly noncalibrated QSOs and SNe Ia, we obtain that w is always consistent within 1σ with $w = -1$ if Ω_M is fixed to 0.3 (as expected in a flat Λ CDM model), independently of the treatment of the correction for evolution. Instead, when also varying Ω_M , we obtain $w \sim -1.6$ and $\Omega_M \sim 0.46$ without correction, $w \sim -0.7$ and $\Omega_M \sim 0.06$ with a fixed correction, even if in this last case Ω_M does not converge, and $w \sim -1.2$ and $\Omega_M \sim 0.36$ with a correction that varies with the cosmological parameters. This last case is compatible with $\Omega_M = 0.3$ and $w = -1$ within 2σ . The results presented for the flat Λ CDM model on the values of g , b , and sv are once again valid in this case of a flat w CDM model. This strongly stresses the independence of the parameters of the RL relation on the assumed cosmological model.

5.5. Impact on the H_0 Tension

We also would like to stress that if we consider noncalibrated QSOs + SNe, both with H_0 and Ω_M changing together or only changing H_0 , then we can safely state that the resulting H_0 values are all compatible with each other, and they are between

the values of H_0 determined by the Planck collaboration and those of the SNe Ia. This result is very intriguing since it is similar to the results obtained by Freedman (2021; see their Figures 10 and 11). In Freedman (2021), the authors use a different methodology due to a local characteristic of the red giants. Their approach follows the traditional, cosmic-ladder treatment, which means that distant objects such as SNe Ia are calibrated by nearby standard candles such as tip of the red giant branch. In this approach, H_0 is determined for nearby objects (i.e., redshift of the objects is much smaller than 1), for which the luminosity distance mainly depends on H_0 and z only and does not depend on other cosmological parameters such as Ω_M and Ω_Λ . In that sense, Freedman's approach is different from our new approach that overcomes the circularity problem where H_0 is obtained simultaneously with other cosmological parameters. Those results could imply that the Hubble constant tension could be due to observational biases, but one needs to have a larger sample to verify such a hypothesis (Freedman 2021). When we consider the QSOs alone but calibrated with SNe Ia, we have mixed results about the H_0 values. If we consider that the evolutionary function for Ω_M provides the most reliable estimates, then we can conclude that values closer to the Planck results are the most favored. On the other hand, from their Figure 11, we can still learn that when we vary only one cosmological parameter at time, again the results are mixed. Indeed, if we consider only H_0 varying without evolution, then we have compatibility for H_0 with SNe Ia, while when we fix the evolution, the H_0 value lies between the values obtained by CMB and SNe Ia. From this analysis, we still cannot conclude that evolution is the driving factor that pushes H_0 closer to the Planck values. Indeed, for the case of both parameters free to vary, the results with and without evolution lie on the opposite side of the Planck (no evolution) and SNe Ia values for H_0 (for fixed evolution). We also would like to stress that the H_0 trend toward the value of $70 \text{ km s}^{-1} \text{ Mpc}^{-1}$ may also stem from the fact that SNe Ia are uncalibrated (namely, calibrated arbitrarily for an absolute magnitude $M = -19.35$ and thus consequently at $H_0 = 70 \text{ km s}^{-1} \text{ Mpc}^{-1}$, see also Perivolaropoulos & Skara 2023); thus, the trend may not stem from the underlying physics, but from this calibration choice (A. Riess, private communication). Notwithstanding the importance of this discussion, this topic is beyond the scope of the current paper, and we will address it more in detail in a forthcoming publication.

In order to verify these results statistically, due to a large uncertainty of the parameters in cases with calibrated QSOs, we have run the Monte Carlo simulations 100 times to better evaluate the uncertainties and the true value of the cosmological parameters. The achieved distributions of the values of the H_0 obtained in looped computations are shown in Figure 5, and the mean values are presented in Table 3. This approach has been already successfully used for GRBs in Dainotti et al. (2023), and here we show the histograms of the distributions of H_0 for the five cases that are detailed in the lower part of Table 3.

6. Summary and Conclusions

In this work, we analyzed the flat and nonflat Λ CDM models and the flat w CDM model using SNe Ia and the most updated sample of QSOs, as cosmological probes in view of testing QSOs as distance indicators and alleviating the H_0

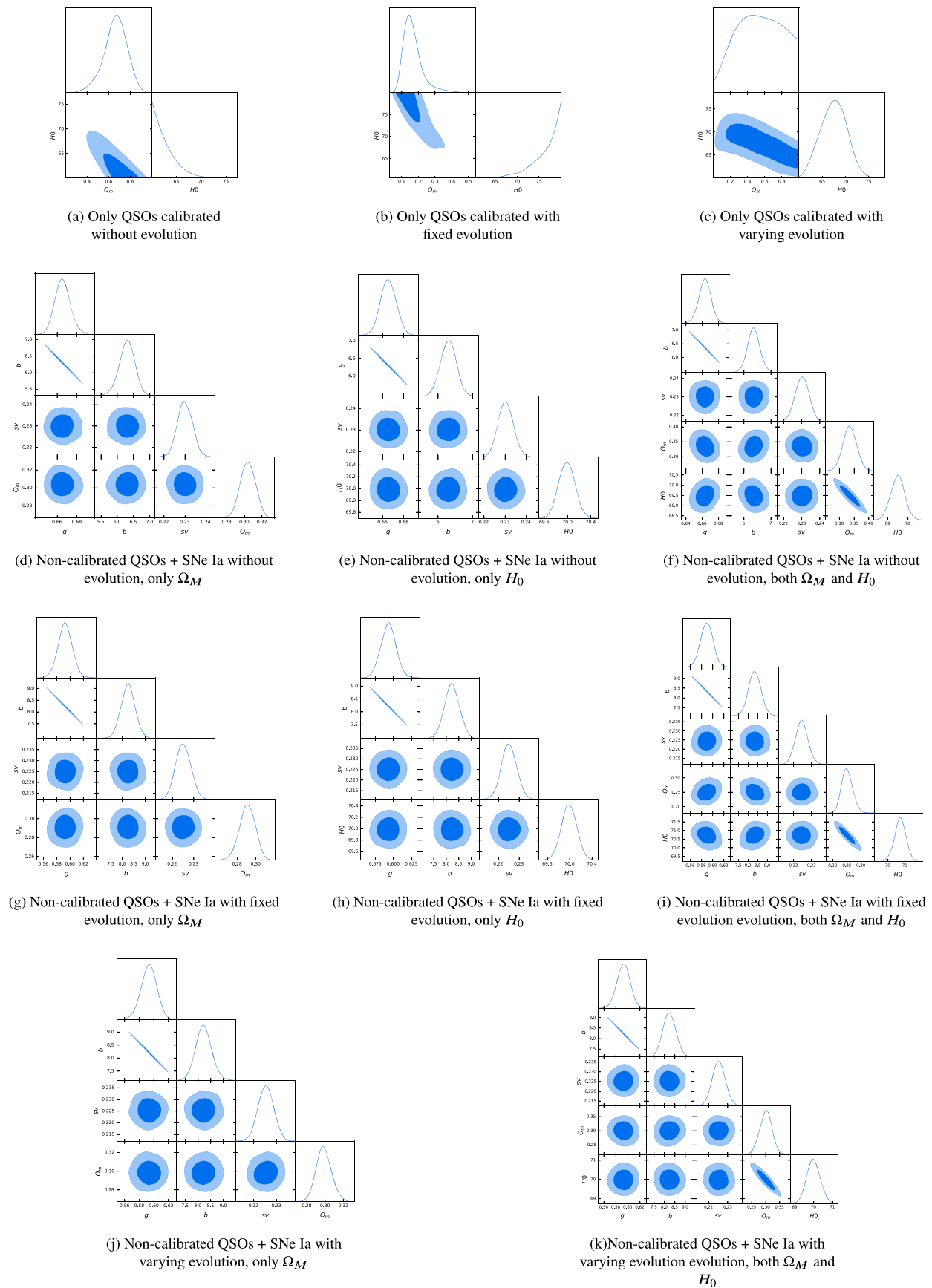


Figure 6. Corner plots obtained under the assumption of the flat Λ CDM model.

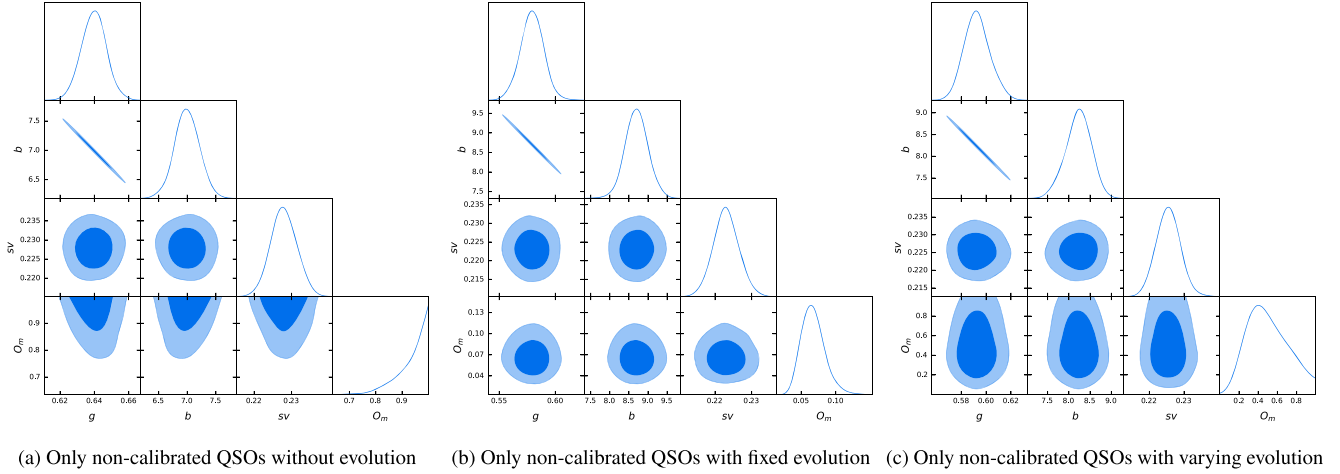


Figure 7. Corner plots obtained under the assumption of the flat Λ CDM model using noncalibrated QSOs alone.

tension issue. This study is strongly motivated by the need for testing the predictions of the spatially flat Λ CDM model and searching for possible deviations to explain the theoretical and observational shortcomings of this model, both in the direction of a nonflat universe and of a potential new physics. The inclusion of QSOs in the cosmological analysis is crucial to this aim as they extend the Hubble–Lemaître diagram of SNe Ia up to a higher redshift range ($z = 2.26–7.54$) in which predictions from different cosmological models can be better distinguished and more easily compared to observational data. We explored and compared different approaches to apply the RL relation for including QSOs in the cosmological analyses. Specifically, we used this relation both in its original form and with luminosities corrected for selection biases and evolution in redshift. In this latter approach, making use of the EP method, we investigated both a fixed evolution and an evolution that depends on the cosmological parameters of the model studied to overcome the circularity problem. The latter technique has recently been applied to GRBs (Dainotti et al. 2023), but this is the first time in the literature that it has been used for QSOs. This study also addresses some previous criticisms concerning the application of the X–UV relation in cosmology (e.g., Petrosian et al. 2022). All of these approaches have also been explored using both noncalibrated QSOs combined with SNe Ia and QSOs alone calibrated with SNe Ia. Below, we summarize our main results.

1. In the effort to overcome the circularity problem, we apply the innovative method in which the correction of luminosities for the evolution in redshift varies together with the cosmological parameters of the assumed cosmological model. Our investigation proves that k_{L_X} and $k_{L_{UV}}$ significantly depend on the cosmological parameters, as shown in Figures 3 and 4. Assuming a nonflat Λ CDM model with $\Omega_M = 0.3$, the values of k do not vary much for Ω_k close to $\Omega_k = 0$, being compatible within 1σ with the value obtained for $\Omega_k = 0$ up to $\Omega_k \sim -0.4$ for both UV and X-ray wavelengths (upper row of Figure 4). Moreover, if we consider the whole parameter space (i.e., $k(\Omega_M, \Omega_k)$ in the upper row of Figure 3), we conclude that, in reasonable regions of this space, the values of k are compatible with those obtained for $\Omega_k = 0$, $\Omega_M = 0.3$ for both UV and X-ray cases.

Similar conclusions can be drawn for $k(w)$ and $k(\Omega_M, w)$ in the flat w CDM model. Indeed, if we fix $\Omega_M = 0.3$, k values are compatible with those obtained with $w = -1$ in the whole range of w explored, as shown in the bottom row of Figure 4 for both the UV and X-ray cases. This explains why we do not observe any significant differences in the cosmological results between the computation of w with fixed correction for evolution and that with $k = k(w)$ (see Table 1). As happens for the nonflat Λ CDM case, k values in the parameter space $\{\Omega_M, w\}$ result are compatible within 2σ with those obtained for $\Omega_M = 0.3$ and $w = -1$ for both UV and X-ray cases (see bottom row of Figure 3). Nevertheless, since we explore the behavior of k in very wide ranges of the cosmological parameters Ω_M , Ω_k , and w , we do observe significant deviation ($>3\sigma$) of k values from that expected for $\Omega_M = 0.3$, $\Omega_k = 0$, and $w = -1$ in some extreme regions of the parameter spaces. Thus, in these particular regions, although one may argue the need of exploring such exotic parameter space, the dependence of k on the cosmological parameters is significant and should be taken into account in the computations.

2. Under the assumption of a flat Λ CDM model, results from QSOs alone calibrated with SNe Ia (the left side of Table 1 and Figures 6(a)–(c)) do not show a common trend, with values of Ω_M and H_0 that have large uncertainties, span a wide range of values, and are not well constrained. These issues are completely removed by joining noncalibrated QSOs and SNe Ia in the analyses. Indeed, with this sample, we do not encounter any convergence issue and, in addition, we always find a common trend toward $\Omega_M = 0.3$ and $H_0 = 70$ that becomes tighter (within 1σ), with the application of a correction for the evolution in the redshift of luminosities that varies together with the cosmological parameters (see the right side of Table 1 and Figures 6(j) and (k)). Within this model, considering the data set of QSOs alone not calibrated on SNe Ia and fixing $H_0 = 70 \text{ km s}^{-1} \text{ Mpc}^{-1}$, presents interesting results on the Ω_M parameter (see Table 2 and Figure 7). More specifically, this investigation also shows that QSOs alone, without any calibration, well constrain Ω_M once we include a correction for the evolution with redshift that varies with the cosmological parameter (i.e., $k = k(\Omega_M)$). This case

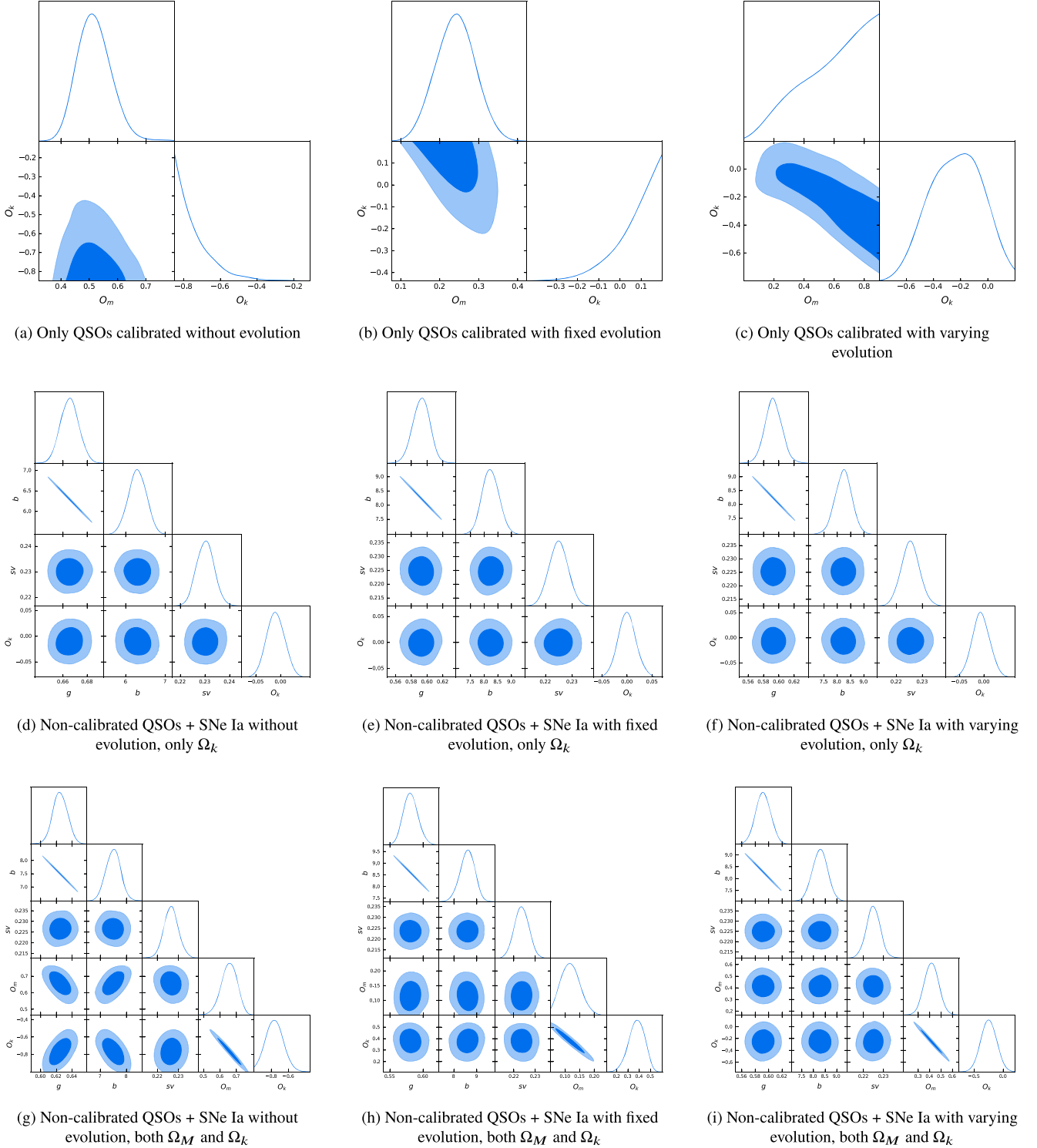


Figure 8. Corner plots obtained under the assumption of the nonflat Λ CDM model.

results in Ω_M compatible within 1σ with $\Omega_M=0.3$, but with a preference toward higher values.

- When allowing for a possible curvature of the universe, QSOs calibrated alone present, as in the previous case, some convergence issues. Nevertheless, when considering a fixed correction for evolution and both Ω_M and Ω_k as free cosmological parameters of the fit, we obtain Ω_M compatible with $\Omega_M=0.3$ within 2σ . These results are shown on the left side of Table 1 and Figures 8(a)–(c).

When fitting together QSOs that are noncalibrated and SNe Ia (the right side of Table 1 and Figures 8(d)–(i)), Ω_k remains compatible within 1σ with $\Omega_k=0$ if we fix $\Omega_M=0.3$, both correcting and not correcting for the evolution. However, Ω_k approaches very different values once Ω_M is free to vary.

- Assuming a flat w CDM model, calibrated QSOs alone do not clearly distinguish between the quintessence and the phantom DE scenario, as shown in the left side of Table 1

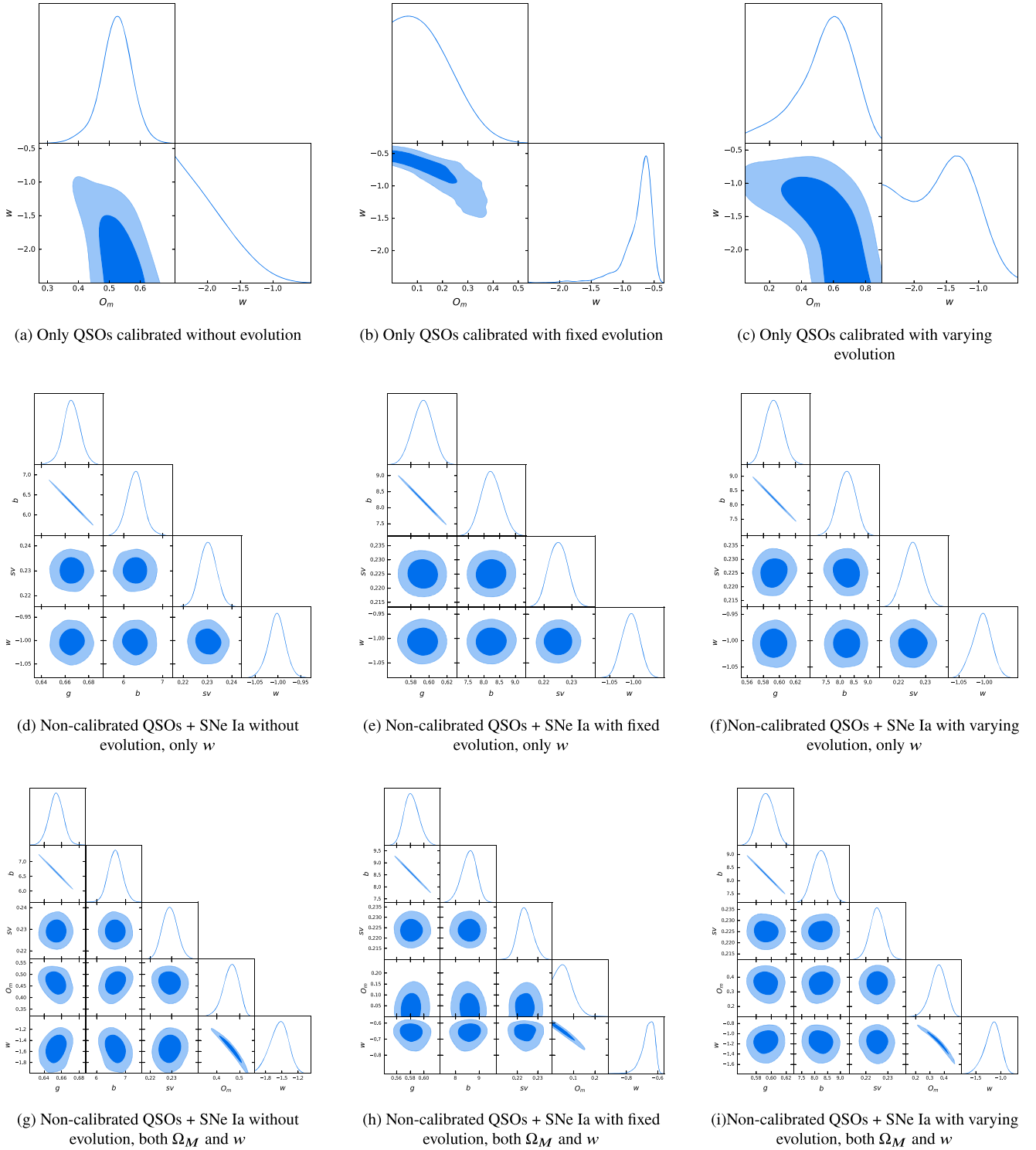


Figure 9. Corner plots obtained under the assumption of the w CDM model.

and in Figures 9(a)–(c). Instead, when considering noncalibrated QSOs together with SNe Ia, in all cases, we obtain compatibility in 1σ with $w = -1$ when $\Omega_M = 0.3$ (as expected in a flat Λ CDM scenario), while also varying Ω_M results in significant deviations from $w = -1$, except for the case with a correction that varies with the cosmological parameters, in which we recover compatibility in 2σ with $\Omega_M = 0.3$ and $w = -1$. This is shown in the right side of Table 1 and in Figures 9(d)–(i).

5. Investigating the results on the parameters of the RL relation when the QSO sample is not calibrated, we obtain that, by comparing cases with the same treatment of the correction for evolution, the fitted values of g , b , and sv are always the same, independently of the cosmological model assumed and cosmological results obtained. Indeed, in our cosmological computations, we do not obtain any significant correlation of the parameters of the RL relation with the cosmological ones, as is

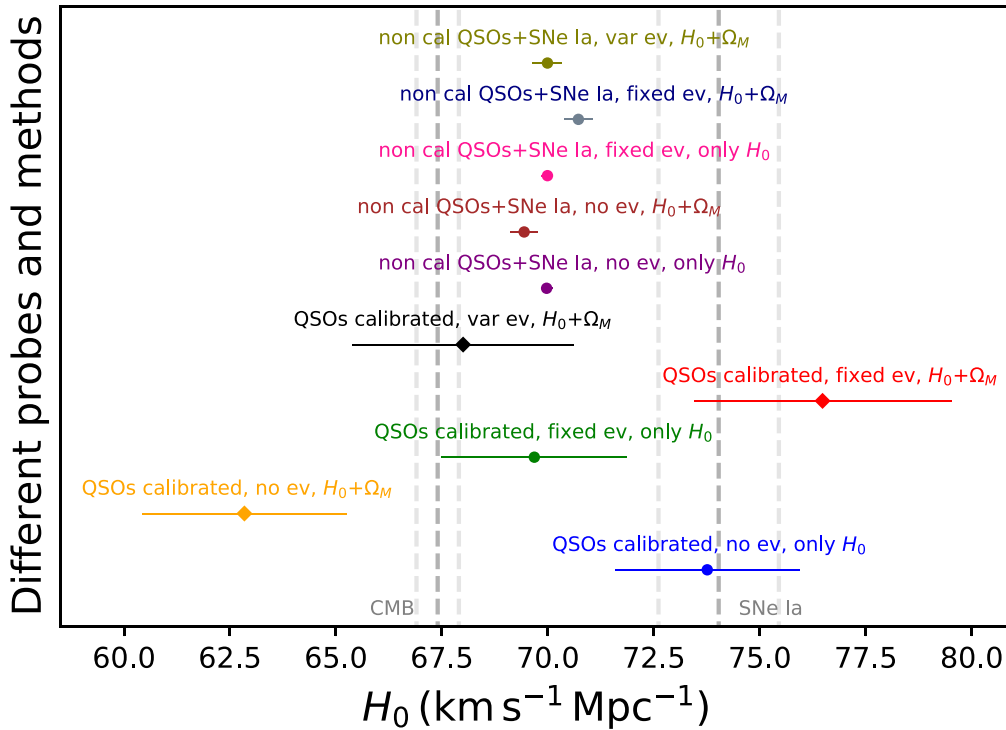


Figure 10. Comparison between the values of H_0 obtained in all of our analyses. Beside each point, we report both the corresponding data set and methodology used for the computation and the z_s -score with respect to the H_0 value obtained from the CMB, defined as $z_s = \frac{|H_{0,\text{CMB}} - H_0|}{\sqrt{\sigma_{H_0,\text{CMB}}^2 + \sigma_{H_0}^2}}$, where H_0 refers to the value obtained from our fit. The two vertical dashed gray lines with the corresponding dashed light-gray lines are the reference points of CMB and SNe Ia measurements with their 1σ uncertainties. The points marked with “◆” correspond to the cases in which the analyses do not converge for one or more parameters.

visible in Figures 6–9. In addition, the application of the correction for the evolution, both fixed and free to vary with the cosmological parameters, reduces the intrinsic dispersion of the relation by a factor of 0.022 (from $sv = 0.230$ to $sv = 0.225$) making the RL relation even stronger.

6. Focusing on how the H_0 tension is impacted by our analyses, we show in Figure 10 the H_0 values with their corresponding 1σ uncertainties obtained in all of the cases studied in this work. These values can be compared to the reference measurements from SNe Ia ($H_0 = 74.03 \pm 1.42 \text{ km s}^{-1} \text{ Mpc}^{-1}$) and CMB ($H_0 = 67.4 \pm 0.5 \text{ km s}^{-1} \text{ Mpc}^{-1}$), shown with vertical dashed gray lines. Beside each point, we also report the computed z_s -score with respect to the CMB. This is defined as $z_s = \frac{|H_{0,\text{CMB}} - H_0|}{\sqrt{\sigma_{H_0,\text{CMB}}^2 + \sigma_{H_0}^2}}$, where $H_{0,\text{CMB}} = 67.4$, $\sigma_{H_0,\text{CMB}} = 0.5$, and H_0 and σ_{H_0} refer to the value and 1σ error obtained from our fit, respectively. This computation allows us to compare each of the case results with that obtained from the CMB. Referring to Figure 10 and to Table 1, we note that the 1σ errors on H_0 strongly decrease when we consider noncalibrated QSOs combined with SNe Ia, compared to the cases with calibrated QSOs alone, due to the significant contribution of SNe Ia. Indeed, the inclusion of SNe Ia in the cosmological computations guarantees tighter constraints on the free cosmological parameters, also removing convergence issues that are instead present when we do not consider the SNe Ia sample. In addition, calibrated QSOs alone do not show any precise hint of the H_0 favored value, as the best-fit values span a very wide range of values, even from

values lower than that of the CMB to values greater than that of SNe Ia (blue, orange, green, red, and black points). Conversely, all of the H_0 values obtained with noncalibrated QSOs combined with SNe Ia (purple, brown, pink, dark blue, and olive points) are compatible within 2σ with each other, pointing clearly to the region intermediate between that of the CMB and SNe Ia, with a z_s -score that increases significantly. Notably, the 1σ uncertainties on H_0 obtained with noncalibrated QSOs together with SNe Ia are even smaller than $\sigma_{H_0,\text{CMB}} = 0.5$, reaching a value of $\sigma_{H_0} = 0.14$ in the case with a fixed correction for evolution with H_0 , the only free parameter of the fit. These results, concerning both the H_0 value and its uncertainty, prove the possible strong impact of our work on the H_0 tension. In light of the newest results of binned analysis of the SNe Ia sample (Dainotti et al. 2021b) and SNe Ia together with BAOs (Dainotti et al. 2022b) showing the existence of an evolution of the H_0 parameter with redshift, our results underscore the significance of studying such a model, as high-redshift QSOs could be shown more clearly if such an evolution exists, and as the model could explain the current H_0 tension problem.




In conclusion, among all of the data sets and methodologies investigated in this work, the case with noncalibrated QSOs combined with SNe Ia and with the correction for the evolution in redshift of luminosities varying together with the cosmological parameters is the one that turned out to be the most reliable and complete, as expected. Indeed, including the SNe Ia sample and taking into account this type of redshift evolution removes convergence issues and results in tighter constraints

on the fitted parameters in all cosmological models studied, also allowing us to overcome the circularity problem. Considering this case, our results are always compatible with a flat Λ CDM model with $\Omega_M=0.3$ and $H_0=70 \text{ km s}^{-1} \text{ Mpc}^{-1}$, without any hint of a DE with $w \neq -1$ nor a nonflat universe. More precisely, we always have compatibility in 1σ , except for two cases: the flat w CDM and the nonflat Λ CDM models in which both cosmological parameters are free to vary, showing a 2σ discrepancy from $\Omega_M=0.3$ and $w=-1$, and from $\Omega_M=0.3$ and $\Omega_k=0$, respectively. We note that our approach has led to values of cosmological parameters closer to those obtained with SNe Ia alone (assuming a flat Λ CDM model) than those presented in the QSO literature. In addition, this case also allowed us to investigate how the values of the parameters of the RL relation are impacted by the assumption of a specific model. About this, we have strongly proved that these parameters do not show any dependence on the choice of the cosmological model.

This article shows that, when it comes to cosmological measurements, one should be extremely careful in assuming the absence of selection biases and redshift evolution. Indeed, it is necessary to study their possible presence and behavior, as corrections for such effects can push the constraint of cosmological parameters further. Future analyses should investigate those biases also for other probes, such as SNe Ia. We showed that QSOs alone can be used as standalone probes without any cut in redshift or calibration, once the correction for the evolution is accounted for. Indeed, for the first time in the literature for such a sample, we have obtained closed contours in 2σ for the computation of Ω_M . In the end, this work could represent a leap forward in shedding light on the H_0 tension and investigating if the current tension could be ascribed to an evolution of H_0 with redshift or to a constant H_0 value that stands between that of SNe Ia and CMB.

A.L. would like to acknowledge the financial support from the Programme Council of Studies in Mathematics and the Natural Sciences (SMP) at the Jagiellonian University. S.N. is supported financially by JSPS KAKENHI (A) grant No. JP19H00693, Interdisciplinary Theoretical and Mathematical Sciences Program (iTHEMS), and the Pioneering Program of RIKEN for Evolution of Matter in the Universe (r-EMU). G.B. acknowledges the Istituto Nazionale di Fisica Nucleare (INFN), sezione di Napoli, for supporting her visit at NAOJ. G.B. is grateful to have been hosted by the Division of Science. M.G. D. acknowledges the Division of Science and NAOJ.

ORCID iDs

Giada Bargiacchi  <https://orcid.org/0000-0002-0167-8935>
 Maria Giovanna Dainotti  <https://orcid.org/0000-0003-4442-8546>
 Salvatore Capozziello  <https://orcid.org/0000-0003-4886-2024>

References

Alam, S., Aubert, M., Avila, S., et al. 2021, *PhRvD*, 103, 083533
 Avni, Y., & Tananbaum, H. 1986, *ApJ*, 305, 83
 Bañados, E., Venemans, B. P., Mazzucchelli, C., et al. 2018, *Natur*, 553, 473
 Bargiacchi, G., Benetti, M., Capozziello, S., et al. 2022, *MNRAS*, 515, 1795
 Bargiacchi, G., Risaliti, G., Benetti, M., et al. 2021, *A&A*, 649, A65
 Benetti, M., & Capozziello, S. 2019, *JCAP*, 12, 008
 Bisogni, S., Lusso, E., Civano, F., et al. 2021, *A&A*, 655, A109
 Capozziello, S., Benetti, M., & Spallicci, A. D. A. M. 2020, *FoPh*, 50, 893

Capozziello, S., & D'Agostino, R. 2020, *MNRAS*, 494, 2576
 Capozziello, S., D'Agostino, R., & Luongo, O. 2019, *IJMPD*, 28, 1930016
 Cardone, V. F., Capozziello, S., & Dainotti, M. G. 2009, *MNRAS*, 400, 775
 Cardone, V. F., Dainotti, M. G., Capozziello, S., & Willingale, R. 2010, *MNRAS*, 408, 1181
 Carroll, S. M. 2001, *LRR*, 4, 1
 Carroll, S. M., Press, W. H., & Turner, E. L. 1992, *ARA&A*, 30, 499
 Colgáin, E. Ó., Sheikh-Jabbari, M. M., Solomon, R., et al. 2022, arXiv:2203.10558
 D'Agostini, G. 2005, arXiv:physics/0511182
 Dainotti, M., Lenart, A., Sarracino, G., et al. 2020a, *ApJ*, 904, 97
 Dainotti, M., Levine, D., Fraija, N., & Chandra, P. 2021a, *Galax*, 9, 95
 Dainotti, M., Petrosian, V., Willingale, R., et al. 2015, *MNRAS*, 451, 3898
 Dainotti, M. G., Bargiacchi, G., Lenart, A., et al. 2022a, *ApJ*, 931, 106
 Dainotti, M. G., Cardone, V. F., & Capozziello, S. 2008, *MNRAS*, 391, L79
 Dainotti, M. G., Cardone, V. F., Piedipalumbo, E., & Capozziello, S. 2013a, *MNRAS*, 436, 82
 Dainotti, M. G., De Simone, B., Schiavone, T., et al. 2021b, *ApJ*, 912, 150
 Dainotti, M. G., De Simone, B. D., Schiavone, T., et al. 2022b, *Galax*, 10, 24
 Dainotti, M. G., Lenart, A. L., Chraya, A., et al. 2023, *MNRAS*, 518, 2201
 Dainotti, M. G., Livermore, S., Kann, D. A., et al. 2020b, *ApJL*, 905, L26
 Dainotti, M. G., Nagataki, S., Maeda, K., Postnikov, S., & Pian, E. 2017, *A&A*, 600, A98
 Dainotti, M. G., Nielson, V., Sarracino, G., et al. 2022c, *MNRAS*, 514, 1828
 Dainotti, M. G., Ostrowski, M., & Willingale, R. 2011, *MNRAS*, 418, 2202
 Dainotti, M. G., Petrosian, V., & Bowden, L. 2021c, *ApJL*, 914, L40
 Dainotti, M. G., Petrosian, V., Singal, J., & Ostrowski, M. 2013b, *ApJ*, 774, 157
 Dainotti, M. G., Sarracino, G., & Capozziello, S. 2022d, *PASJ*, 74, 1095
 Di Valentino, E., Melchiorri, A., & Silk, J. 2020, *NatAs*, 4, 196
 Di Valentino, E., Melchiorri, A., & Silk, J. 2021, *ApJL*, 908, L9
 Efron, B., & Petrosian, V. 1992, *ApJ*, 399, 345
 Evans, I. N., Primini, F. A., Glottfelty, K. J., et al. 2010, *ApJS*, 189, 37
 Freedman, W. L. 2021, *ApJ*, 919, 16
 Gonzalez, J. E., Benetti, M., von Martens, R., & Alcaniz, J. 2021, *JCAP*, 2021, 060
 Handley, W. 2021, *PhRvD*, 103, L041301
 Just, D. W., Brandt, W. N., Shemmer, O., et al. 2007, *ApJ*, 665, 1004
 Khadka, N., & Ratra, B. 2020a, *MNRAS*, 492, 4456
 Khadka, N., & Ratra, B. 2020b, *MNRAS*, 497, 263
 Khadka, N., & Ratra, B. 2021, *MNRAS*, 502, 6140
 Khadka, N., & Ratra, B. 2022, *MNRAS*, 510, 2753
 Kluyver, T., Ragan-Kelley, B., Pérez, F., et al. 2016, in Positioning and Power in Academic Publishing: Players, Agents and Agendas, ed. F. Loizides & B. Schmidt (Amsterdam: IOS Press), 87
 Lusso, E., Comastri, A., Vignali, C., et al. 2010, *A&A*, 512, A34
 Lusso, E., Piedipalumbo, E., Risaliti, G., et al. 2019, *A&A*, 628, L4
 Lusso, E., & Risaliti, G. 2016, *ApJ*, 819, 154
 Lusso, E., & Risaliti, G. 2017, *A&A*, 602, A79
 Lusso, E., Risaliti, G., Nardini, E., et al. 2020, *A&A*, 642, A150
 Menzel, M. L., Merloni, A., Georgakakis, A., et al. 2016, *yCat*, J/MNRAS/457/110
 Moresco, M., Amati, L., Amendola, L., et al. 2022, arXiv:2201.07241
 Nardini, E., Lusso, E., Risaliti, G., et al. 2019, *A&A*, 632, A109
 Páris, I., Petitjean, P., Aubourg, É., et al. 2018, *A&A*, 613, A51
 Park, C. -G., & Ratra, B. 2019, *ApJ*, 882, 158
 Peebles, P. J. E. 1984, *ApJ*, 284, 439
 Perivolaropoulos, L. 2014, *Galax*, 2, 22
 Perivolaropoulos, L., & Kazantzidis, L. 2019, *IJMPD*, 28, 1942001
 Perivolaropoulos, L., & Skara, F. 2021, *PhRvD*, 104, 123511
 Perivolaropoulos, L., & Skara, F. 2022, *Univ*, 8, 502
 Perivolaropoulos, L., & Skara, F. 2023, arXiv:2301.01024
 Perlmutter, S., Aldering, G., Goldhaber, G., et al. 1999, *ApJ*, 517, 565
 Petrosian, V., Singal, J., & Mutchnick, S. 2022, *ApJL*, 935, L19
 Planck Collaboration, Aghanim, N., Akrami, Y., et al. 2020, *A&A*, 641, A6
 Postnikov, S., Dainotti, M. G., Hernandez, X., & Capozziello, S. 2014, *ApJ*, 783, 126
 Richards, G. T., Strauss, M. A., Fan, X., et al. 2006, *AJ*, 131, 2766
 Riess, A. G., Filippenko, A. V., Challis, P., et al. 1998, *AJ*, 116, 1009
 Riess, A. G., Macri, L., Li, W., et al. 2009, *ApJS*, 183, 109
 Risaliti, G., & Lusso, E. 2015, *ApJ*, 815, 33
 Risaliti, G., & Lusso, E. 2019, *NatAs*, 3, 272
 Rodney, S. A., Riess, A. G., Scolnic, D. M., et al. 2015, *AJ*, 150, 156
 Salvestrini, F., Risaliti, G., Bisogni, S., Lusso, E., & Vignali, C. 2019, *A&A*, 631, A120
 Sandage, A., Saha, A., Tammann, G. A., et al. 1996, *ApJL*, 460, L15

- Scolnic, D. M., Jones, D. O., Rest, A., et al. 2018, *ApJ*, 859, 101
- Singal, J., George, J., & Gerber, A. 2016, *ApJ*, 831, 60
- Singal, J., Petrosian, V., Lawrence, A., & Stawarz, L. 2011, *ApJ*, 743, 104
- Steffen, A. T., Strateva, I., Brandt, W. N., et al. 2006, *AJ*, 131, 2826
- Tananbaum, H., Avni, Y., Branduardi, G., et al. 1979, *ApJL*, 234, L9
- Visser, M., & Barcelo, C. 2000, COSMO-99, International Workshop on Particle Physics and the Early Universe (Singapore: World Scientific), 98
- Vito, F., Brandt, W. N., Bauer, F. E., et al. 2019, *A&A*, 630, A118
- Wang, F., Yang, J., Fan, X., et al. 2021, *ApJL*, 907, L1
- Watson, M. G., Auguères, J. L., Ballet, J., et al. 2001, *A&A*, 365, L51
- Webb, N. A., Coriat, M., Traulsen, I., et al. 2020, *A&A*, 641, A136
- Wolfram Research, Inc. 2021, Mathematica, v13.0.0, <https://www.wolfram.com/mathematica>
- Yang, W., Pan, S., Di Valentino, E., Mena, O., & Melchiorri, A. 2021, *JCAP*, 2021, 008
- Zamorani, G., Henry, J. P., Maccacaro, T., et al. 1981, *ApJ*, 245, 357